

Photometric Analysis and Modeling of a TESS Object of Interest

April 13, 2022

Emma C. Campbell

A senior thesis submitted to the faculty of
Brigham Young University
in partial fulfillment of the requirements for the degree of
Bachelor of Science

Denise Stephens, Advisor

Department of Physics and Astronomy
Brigham Young University

Copyright © 2022 Emma C. Campbell

All Rights Reserved

ABSTRACT

Photometric Analysis and Modeling of a TESS Object of Interest
April 13, 2022

Emma C. Campbell
Department of Physics and Astronomy, BYU
Bachelor of Science

This thesis explores what kind of object a TESS object of interest could be. Photometric data was collected on 7 separate nights at 5 observatories in 4 different filters, resulting in a total of 10 data sets. In addition to the photometric data, modeling was performed using EXOFASTv2 to help determine what kind of object is producing this drop in brightness. Nine out of the ten photometric light curves display characteristics consistent with a planet, while one light curve shows evidence of an eclipsing binary system. All models show characteristics that are consistent with a transiting planet, including transit shape, transit depth, and object radius. Based on the data presented here, it has been concluded that the object is a transiting planet, but further observations are needed to confirm this conclusion.

Keywords: exoplanets, TESS, transiting planets, Eclipsing Binaries, Transit Modeling

ACKNOWLEDGMENTS

I would like to thank the following people: Dr. Denise Stephens for being my advisor, teaching me everything I know, and trusting me to perform high quality research. Dr. Eric Hintz for setting up, controlling, and maintaining the telescopes at the Eyring Science Center and teaching me valuable research skills. Dr. Benjamin Boizelle for assisting me in the installation and use of IDL. The Physics Department at BYU for providing valuable research opportunities for undergraduate students. Thank you to the other observatories that are mentioned in this thesis, and their willingness to share their data with the rest of the TESS team. Thank you to all of the people, both at BYU and at other observatories that operated the telescopes and collected data for our use. I acknowledge Alex Spencer and Jarrod Hansen for creating and updating the data reduction pipeline, making my job much easier. A huge thank you to Jason Eastman, who not only wrote and maintained the EXOFAST software, but helped me install and troubleshoot the program, allowing me to finish this thesis. Thank you to Steven Johansen for ensuring that EXOFAST was working properly on the computers at BYU. Lastly, thank you to all of my family members, friends, peers, and other people in my life who supported me while completing this thesis.

This research has made use of the NASA Exoplanet Archive, which is operated by the California Institute of Technology, under contract with the National Aeronautics and Space Administration under the Exoplanet Exploration Program.

Contents

Table of Contents	iv
1 Introduction	1
1.1 Planet Detection Methods	1
1.2 The Transiting Exoplanet Survey Satellite	5
1.3 Types of False Positives	6
1.4 TFOP Science Groups	9
2 Data Collection and Preparation	12
2.1 Observations and Observatories	12
2.2 Data Processing	13
2.3 Using AstroImageJ	15
3 Observational Data	21
3.1 BYU data	21
3.2 ExoFop Data	25
4 Modelling with EXOFASTv2	31
4.1 EXOFASTv2	31
4.2 Transit Models	32
5 Results and Discussion	36
5.1 Final Results	36
5.2 Future Observations	37
Appendix A Additional Light Curves	39
Appendix B Additional Transit Models	46
Bibliography	48

Chapter 1

Introduction

1.1 Planet Detection Methods

There are a variety of ways to detect planets that are outside of our solar system. Some detection methods include radial velocity, direct imaging, microlensing and transits. Radial velocity looks for a red or blue shift in the starlight. As a planet orbits around a star, the star also moves slightly creating a shift in its light. This is easiest to detect when there is a very massive planet in the system, as that will increase the observed Doppler shift. Based on the shift seen, we can determine if the shift comes from a planet, and the mass of said planet. Direct imaging is one of the few direct exoplanet detection methods. Just as the name suggests, it involves taking an image of the planet itself. This is incredibly difficult because of the nearby starlight. The star typically saturates our image and we cannot see anything near it, but with clever processing techniques we have been able to image a few planets. This can only be done with planets that are very close to Earth, as the planet needs to have a large enough angular size to be spatially resolved in a telescope.

Microlensing is an application of gravitational lensing. As explained by the theory of General Relativity, the path of a photon can be changed as it travels near a massive object. As the light is

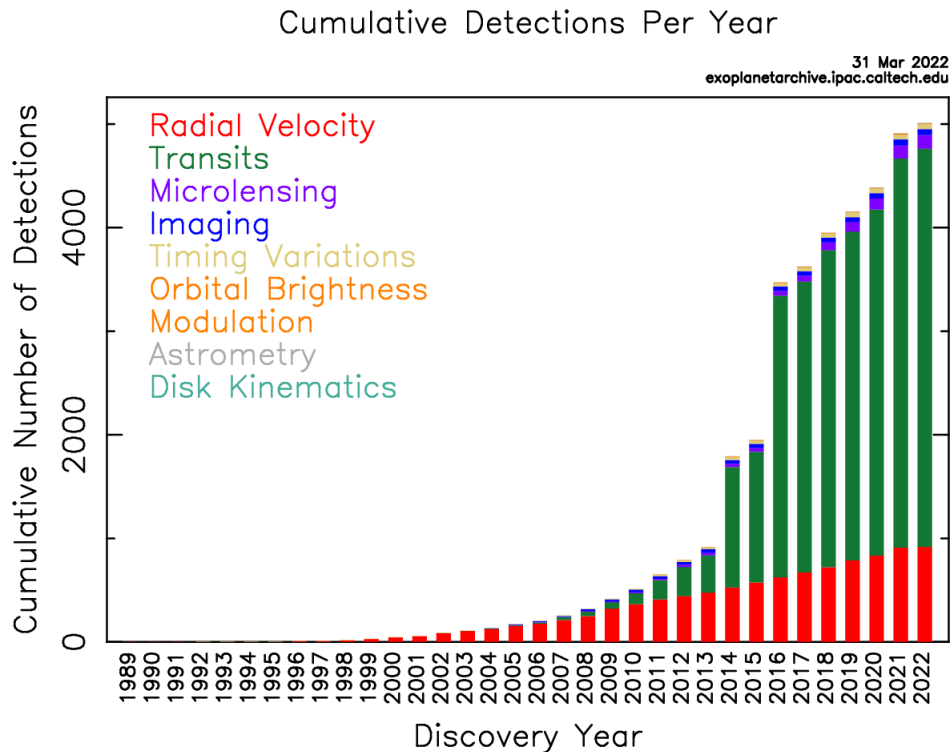


Figure 1.1 The number of exoplanet detections made each year since 1989 with their detection method indicated by color. Current as of April 13, 2022. (Copied From the NASA-Exoplanet-Archive, Accessed April 13, 2022)

bent, it is lensed, making it more intense and easier to observe. In order to detect exoplanets, light from a distant star is observed as it is lensed by another, massive star. If there is an exoplanet orbiting the distant star, then there will be a small period of time in which the overall brightness of the distant star is brighter than expected. The extra intensity is a result of the planet reflecting additional starlight towards the observer. Because this method requires extremely precise measurements, and a near-perfect alignment of two stars it has been one of the least successful planet detection methods.

The rest of this thesis will be focused on the transit method. A transit occurs when the exoplanet in question crosses in front of its host star. When it crosses in front of the star it blocks some of the light from the star, and we are able to detect a small, periodic drop in brightness here on earth. Although all we observe is a small change in light, there are several things we can learn.

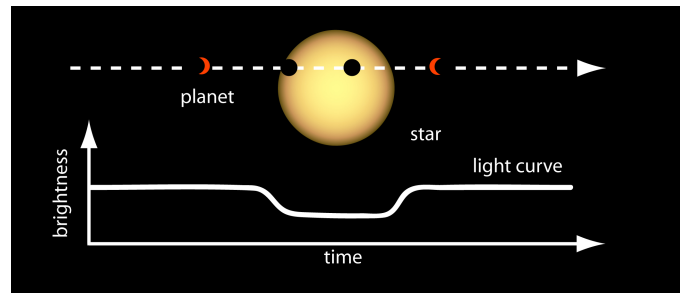


Figure 1.2 An illustration of a transit. As the planet crosses in front the star we detect a small drop in brightness over time. (Copied From NASA-Ames, Accessed May 10, 2021)

The transits happen periodically as the planet orbits its star. The period (P), in conjunction with Newton's version of Kepler's third law, will give us the semi-major axis (a) of the planet.

$$P^2 = \frac{4\pi^2}{G(M_1 + M_2)} a^3$$

As the transit is observed, the depth of the transit is calculated. The depth of the transit equates to the amount of light being blocked, which in turn is proportional to the planet's radius. Then, using the equation,

$$\frac{R_{planet}^2}{R_{star}^2} = Depth$$

the ratio of the planet radius to the star radius can be determined, and the planet radius may be determined if the star's radius is found through other methods such as using a star's spectral type. Most spectral types can easily be found or estimated based on observations in the near infrared. Main sequence stars, like our sun, all have very similar radii, which allows us to use the equation above to estimate the planet's radius. Using the transit depth to get the planet's radius is most successful when the host star is a main sequence star, but can be done with other spectral types as well.

However, there are some limitations and biases associated with the identifying planets using the transit method. In order to view a transit the planet and star must be aligned correctly so that we can see the planet transit from our perspective here on earth. Although there are many planets that fall

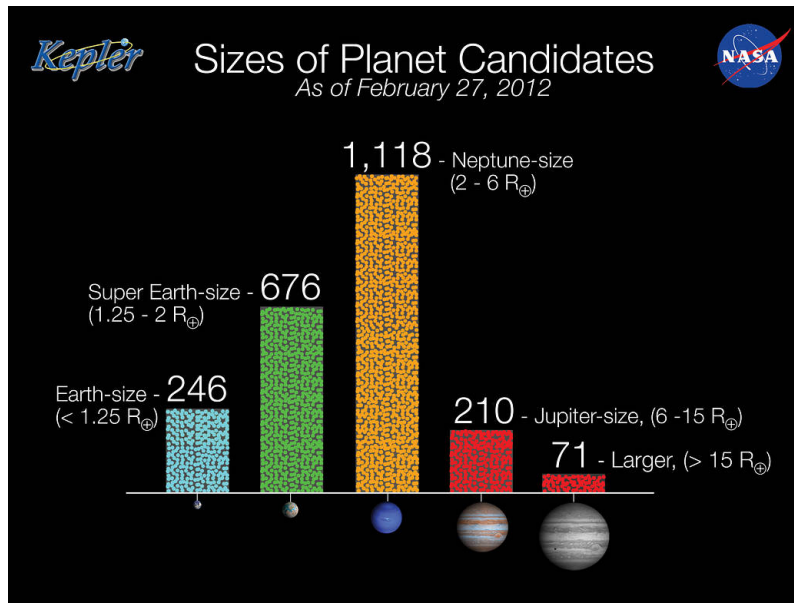


Figure 1.3 A bar graph from the first Kepler data release in 2012, showing the number of planets found and what their rough size it. The most common planet size is a size similar to Neptune (Copied From Nasa-Ames & Wendy Stenzel, Accessed April 10, 2022)

into this category, the transit method is fundamentally limited since not all planetary systems will be oriented correctly for a transit. This detection method also has some observational biases, for instance, it is more likely that a large planet, with a small semi-major axis will be detected since they create a large drop in brightness. This has led to the discovery of a large number of exoplanets called hot Jupiters, which are very large planets that are close to their host star. Even though a large number of hot Jupiters have been discovered, these planets have been found to be rare, statistically speaking. Based on the findings of the Kepler missions, the most common planet size is similar to that of Neptune as seen in figure 1.3 (Batalha et al. 2013). Most of these planets are still very close to their host star, with a typical semi-major axis of less than 1 AU.

All detection methods discussed thus far have their strengths, but also have serious limitations and biases. For instance, the radial velocity method is best for detecting massive planets, and the transit method is best for finding large planets close to the host star. Despite these limitations and biases, transits have been the most successful method thus far, as shown in figure 1.1. This

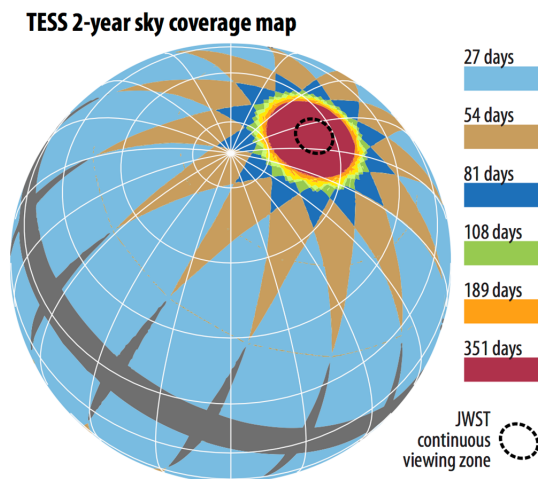


Figure 1.4 The viewing areas of TESS (Copied From the TESS website, Accessed May 10, 2021)

is largely due to the fact that several stars can be monitored at once, where as other methods are only able to monitor one star at a time. This greatly increases the chances of finding an exoplanet, but does not necessarily mean that the transit method is the best method for finding exoplanets. That being said, transits have proven themselves to be an extremely promising exoplanet detection method, resulting in space telescopes, and global, ground based observing effort dedicated to finding transiting exoplanets.

1.2 The Transiting Exoplanet Survey Satellite

TESS (Ricker et al. 2014) is a space telescope that is dedicated to finding transiting exoplanets. As stated in the previous section the transit method relies on exoplanets creating a small, periodic drop in light. TESS observes large portions of the night sky over extended periods of time. TESS observes a hemisphere of the night sky for a full year, and then switches to the other hemisphere for the next year, shown in figure 1.4 This allows TESS to observe most stars for at least 27 days at a time, but can observe some stars for a full year if they are located near the north and south poles.

During these remarkably long observations, TESS is specifically looking for periodic changes in brightness on stars. However, even if TESS successfully finds an object that changes in brightness it does not necessarily mean that it has found a planet. TESS has a large 1440x1440 arcminute field of view, meaning that stars that are within 2.5 arcminutes of each other are extremely difficult to distinguish from each other. As a result, TESS will sometimes attribute a change in brightness to a different, nearby object which needs to be corrected. TESS will also see a drop in flux and assume that it is a transiting planet, when it is actually a different object, such as an eclipsing binary. Eclipsing Binaries are star system where two stars that are orbiting each other, and are in the correct orientation for an observer on Earth can see the two stars eclipse each other. As they eclipse each other a drop in brightness can be observed that is periodic, similar to a transiting planet and can trigger a positive detection. These occasional irregularities necessitate the need for the TESS follow-up observing program (TFOP).

1.3 Types of False Positives

As mentioned, false positives happen on a regular basis (Canas, Accessed April 10, 2022) due to TESS's very large field of view. There are four common types of false positives that occur, as shown in figure 1.5. One of the most common kinds of false positives seen is an eclipsing binary. This can consist of a star and a very small companion star, or a brown dwarf orbiting a star. When there is a small companion star, it can block an amount of light comparable to the light blocked by a planet, but the star is also emitting light. The easiest way to distinguish these systems from an exoplanetary system is through their spectra. When analyzing the spectra of a potential planetary system, only one stellar spectra should be seen, but when there is another star two stellar spectra will be seen superimposed on each other. A star is also more massive than a star, and is typically vetted out by finding the radial velocities of the host star and the small star. The radial velocity

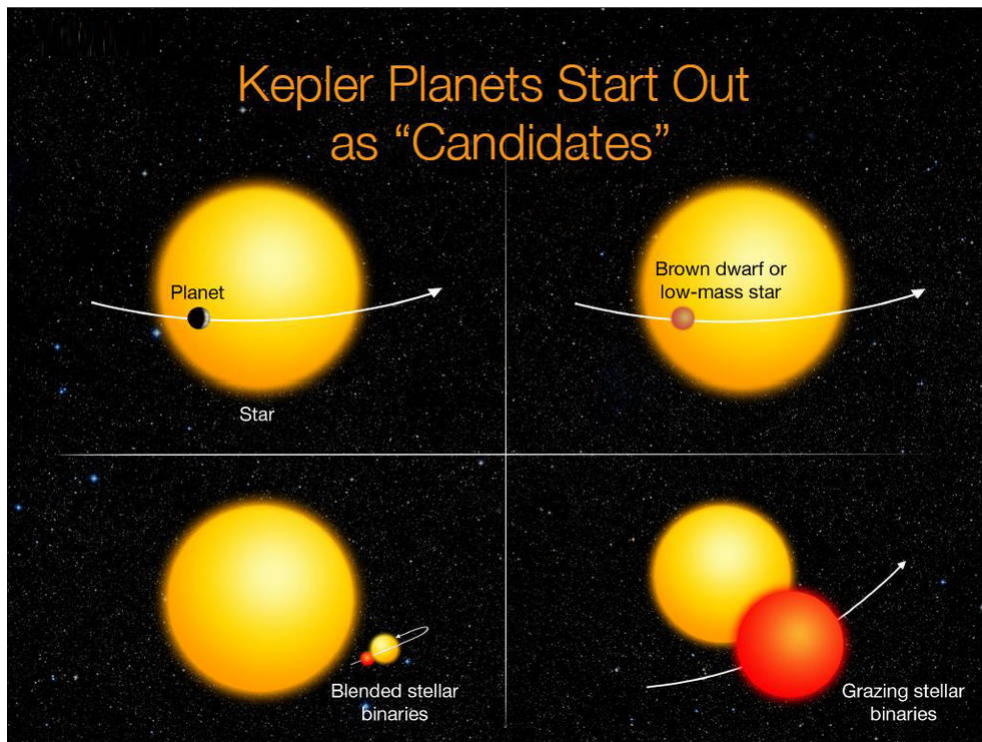


Figure 1.5 This graphic shows some of the systems that are likely to be chosen as candidates. The upper left corner shows the kind of system that TESS is looking for, which is a planet that passes in front of its host star. The upper right corner shows a very common type of candidate that is actually considered a false positive. When a small star is orbiting a larger star it often appears to be a planet, which is why it is a common type of false positive. The lower left corner displays another system that is marked as a candidate, but is actually a blended binary system with multiple stars orbiting each other. The lower right corner shows a grazing binary system, which results in a small drop of light like a transit, but is actually a false positive. This graphic was created for the Kepler mission, but it applies to the TESS mission as well. (Copied from NASA-Ames & Wendy Stenzel, Accessed April 10, 2022)

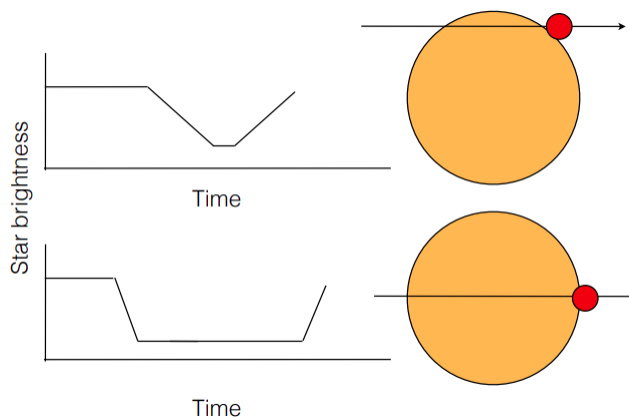


Figure 1.6 The top section shows the shape of a transit that occurs when the planet is only "grazing" the star, and is not passing through the middle. This transit shape is also seen with EB systems. (Copied From Dawson 2020)

gives a mass measurement and can show that the transiting object is too massive to be a planet, and may be another star. A similar process is used to determine if there is a brown dwarf orbiting the host star instead of a planet.

Another common false positive seen is when two stars in an eclipsing binary appear to "graze" each other as they eclipse each other. The stars are oriented in such a way from our perspective on earth that just the edges of the star eclipse each other as they orbit. This results in a drop in light that is comparable to a planet, and is often tagged as a planet candidate by TESS. However, they can be differentiated from an planet fairly easily. In this case the transit has a slightly different shape which is characterized by more gradual slope on the edges of the transit light curve as seen at the top of figure 1.6. This aspect of an eclipsing binary will be explored more in depth in a later section. The spectra for this object will show spectra features from two stars, like discussed above. The radial velocity measurements will also clearly show that the objects are much more massive than a planet, and is hence a star.

The last kind of false positive is a blended binary system, an example of a blended binary is shown in the lower left of figure 1.6. A blended binary is when a smaller binary system is orbiting

a larger star, or there is another combination of stars orbiting each other. Similar to the eclipsing binaries discussed above, these star systems will show periodic changes in light. These systems are easily mistaken for a transiting planet because the drops in the light can be very small due to all of the starlight being emitted, and the ratio of emitted to blocked light is very small, similar to a planet. By using radial velocity, spectroscopic data, and occasionally direct imaging, these objects can be differentiated from transiting planets.

1.4 TFOP Science Groups

TFOP consists of observatories around the world that are part of various science groups that contribute to the TESS mission, as seen in figure 1.7, (Collins et al. 2018). Starting with science group 1 (SG1) (Collins 2019), its role in TFOP is to take ground-based photometric data which, like TESS, looks for changes in flux over time. The main purpose of these observations is to make sure that an object marked by TESS is the source of change in light, or if it is another object nearby such as a nearby eclipsing binary (NEB). Ground-based observations have much smaller fields of view and better angular resolution which allows them to differentiate between the target and other objects that are nearby. SG1 also determines that if the event does occur on the target, that it is a transiting planet and not another type of object that also has changes in flux over time. SG1 also refines parameters for the object, such as transit timing, the depth of the transit, and the length of the transit. All of the observational data presented in this paper comes from observatories that are a part of SG1.

Science group 2 (SG2) specializes in gathering spectroscopic data on the target of interest (Quinn 2019). Spectroscopy is partly used to determine system properties such as mass and velocity, but spectroscopy is also used to help determine whether or not a target is a planet, a binary system, or a false positive. The type of binary system that is found by SG2 is a spectroscopic binary. Spectroscopic binaries are characterized by their large radial velocities, resulting in a large Doppler

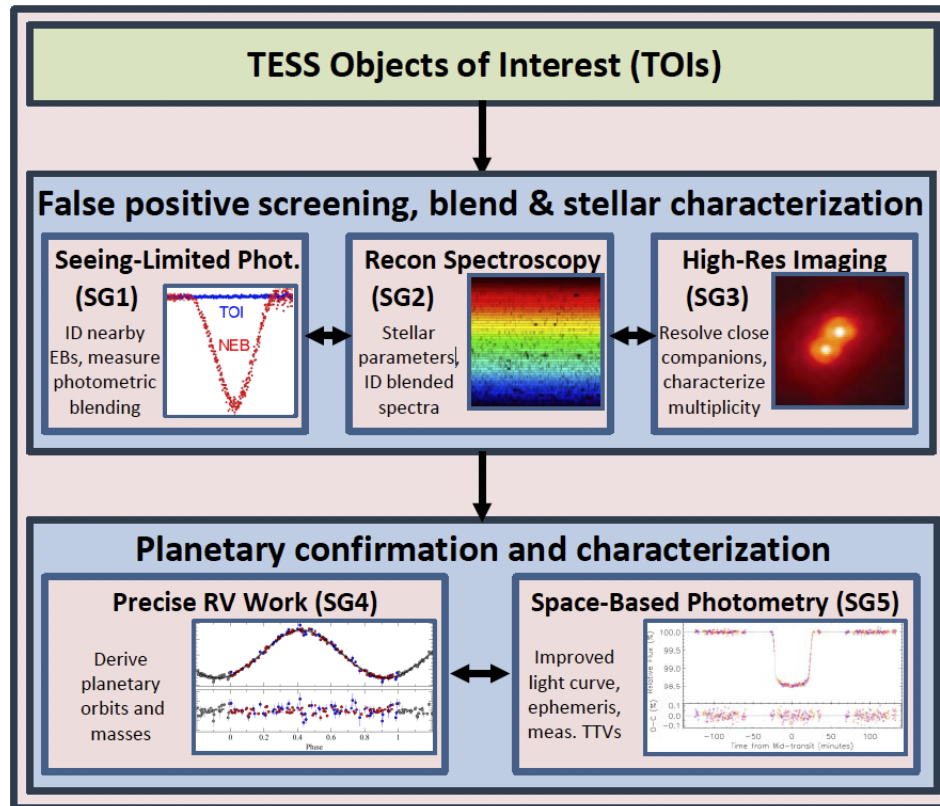


Figure 1.7 A infographic produced by the TESS team at MIT which briefly explains the roles of all science groups that are a part of TFOP (Copied From the TESS website, Accessed May 10, 2021)

shift as the two stars orbit each other. SG2 checks for these large Doppler shifts and radial velocities to check for false positives. SG2 can also detect much smaller radial velocities that could be indicative of a planet orbiting its host star. However, sometimes no radial velocity or Doppler Shift is detected on a target, and that typically means one of two things: the target is not a transiting planet, or it has a very small radial velocity that cannot be detected by SG2. When that is the case, it needs more precise radial velocity measurements and is sent to science group 4 (SG4).

The main goal of SG4 is to derive planetary orbits and masses as it orbits its host star (Latham 2019). The telescopes used by this group are typically very large, expensive, and hard to schedule time on. If a target has been given to SG4 then TFOP is fairly certain that it is a planet based off

the the work from SG1 and SG2, but they cannot get precise enough measurements to derive the planet's properties, and need the high quality telescopes used by SG4. The main goal of this group is to verify that a planet has been detected, and to measure the masses and radii of the planets, especially for planets that have radii smaller than 4 earth radii.

SG3 specializes in high resolution direct imaging of targets of interest (Ciardi 2019). The targets that are given to SG3 are targets that are either a transiting planet, or a very close eclipsing binary. When a binary is very close the light from the two stars can blend together, and we only see a small drop in light, similar to that of a planet. SG3 is able to resolve the target and provide evidence for what kind of object it really is. This is typically accomplished by Keck adaptive optics, as it is one of the few instruments that has a high enough resolution, and advanced instrumentation to resolve these objects. Finally, SG5 makes use of space based telescopes and observatories to confirm or improve upon data that has already been gathered by TESS and TFOP (Dragomir et al. 2019). Since SG5 uses space telescopes, they are able to reduce the uncertainty and find the best possible values for the system's properties. However, since SG5 uses valuable telescope time very few targets are observed by SG5. All of the science groups apart of TFOP are incredibly valuable and play crucial role in the overall TESS mission to find as many exoplanets as possible.

Chapter 2

Data Collection and Preparation

2.1 Observations and Observatories

All data presented in this paper from BYU was collected with the 0.3 meter (12 inch) telescope on the observing deck at the Eyring Science Center on the campus of BYU in Provo, Utah. Four other observatories that are apart of the TFOP team has graciously shared the data that they gathered on this target through the Exoplanet Follow-up Observing Program (ExoFOP) website (Akeson & Christiansen 2019). The four observatories that took data on this target the Las Cumbres McDonald Observatory (LCO-McD)(Brown et al. 2013) in Texas, the Villa '39 Observatory (V39) in California, Observatory de Cal'Ou (Cal'Ou) in Spain and the Private observatory of the Mount (OPM) in France. The specifications for all of these observations are listed in the tables below.

Observatory	Date Obs. (UT)	Diameter (m)	Camera	FOV (arcmin)
BYU	09/06/2020	0.3	FLI ML8300	25.4 x 19
	09/09/2020			
	12/07/2020			
LCO-McD	12/03/2020	1	Sinestro	26.5 x 26.5
V39	08/18/2020	0.35	SX-56 (KAF16803)	32.41 x 32.41
Cal'Ou	11/23/2020	0.4	FLI PL1001	20.7 x 20.7
OPM	10/29/2020	0.2	Atik 383 L+ camera	38 x 29

Observatory	Date Obs. (UT)	Diameter (m)	Filter(s)	Central λ (nm)
BYU	09/06/2020	0.3	Johnson B	436.1
BYU	09/09/2020	0.3	Johnson B	436.1
BYU	12/07/2020	0.3	Johnson B, Sloan z	436.1, 909.7
LCO-McD	12/03/2020	1	Johnson B, Sloan z	436.1, 909.7
V39	08/18/2020	0.35	Cousins I	798
Cal'Ou	11/23/2020	0.4	Johnson B	436.1
OPM	10/29/2020	0.2	Sloan z and g	909.7, 477

(Bessell, 2005), (Fil Accessed April 10, 2022)

2.2 Data Processing

Despite the best efforts of observers, astronomical data always has imperfections. Therefore, data must be calibrated or reduced to mitigate the imperfections before it can be properly analyzed. (Dat Accessed April 10, 2022) For all the data discussed in this paper the standard reduction methods were used.

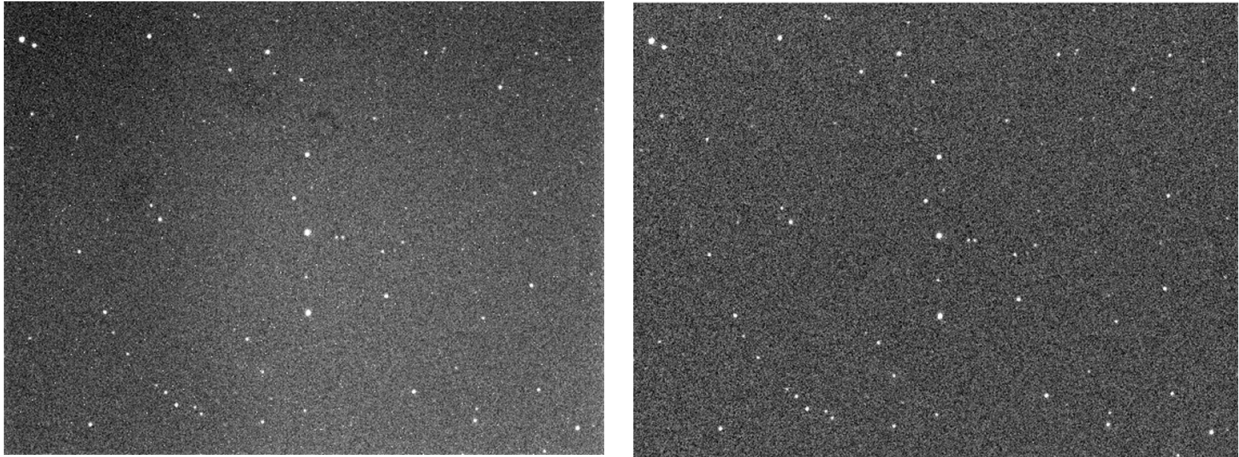


Figure 2.1 The image on the left shows a raw object frame before it has been reduced and calibrated. There are obvious light and dark areas, as well as some faint rings from dust on the mirror. The image on the right is the same object frame after processing. The imperfections in the data have been removed and is now ready to be analyzed.

In addition to the data images, three types of calibration frames are taken at the time of observation. The three types are Biases, Darks, and flats. When using a Charged Coupled Device (CCD) there is a significant amount of readout noise that is introduced when the analog data from the CCD is stored digitally. Because of this it is necessary to introduce a background current. The background current ensures that there is never a negative value on a pixel, and that we do not lose information during the digital readout. A bias frame records the background current so it can be later removed from the astronomical data, but it is crucial to getting accurate and high quality data.

CCDs record the number of electrons that are excited within a pixel. They are typically excited by incoming photons, but can also be excited by thermal energy. Thermal energy is difficult to mitigate, as it requires liquid nitrogen cooling systems to cool the CCD to at least 150 K in order to make the thermal energy negligible. Many observatories do not have liquid nitrogen cooling systems, and are only able to cool the CCD to about 250 K, so the thermal effects must be taken into account. Dark frames are images that are taken with a long exposure time and with the aperture closed. This is to record the thermal effects, which are also called the dark current. Several of these

images are taken, combined, and then subtracted from the object frames. Without dark frames there would be many bright pixels contaminating the image and the data.

Flats are images taken with the same amount of illumination on each pixel. Flat fields are typically taken at twilight when the brightness level of the sky is equal within a telescope's field of view. Flats are necessary for three major reasons: variations in pixel size, dust or other imperfections on mirrors, and for light sources that are off axis and appear dimmer on the CCD. The even illumination allows you to see any brightening or darkening of CCD pixels that are not due to astronomical objects. Flats are then all normalized and then we divide the object frames by the flats since flats are representative of lost flux. Bias and dark frames are combined, and their levels of flux are subtracted from the object frames since they represent extra flux that are from sources other than stars. This step is crucial to ensure that the data is uncontaminated and as accurate as possible. A before and after comparison of an object frame is shown in figure 2.1. At BYU this was done by hand, or through the use of a data reduction pipeline (Spencer Brigham Young University, Provo, UT 2019) written in IRAF (Shames & Tody 1986).

2.3 Using AstroImageJ

Now that the data set has been reduced AstroImageJ (AIJ) (Collins et al. 2017) is employed. AIJ is a program used by many astronomers to perform multi-aperture photometry. One data set typically consists of over 150 images. The images are usually taken every few minutes over a period of 5-6 hours. Throughout that time the filters are changed periodically so there is an equal number of images in all filters. However, some nights the target is only observed in one filter, and in another filter on another night. In addition to the target frames, calibration frames are typically taken on the same night as well. Occasionally calibration frames that were taken on a different night are used to reduce the data, but it is preferred to use calibration frames from the same night. Once a data set

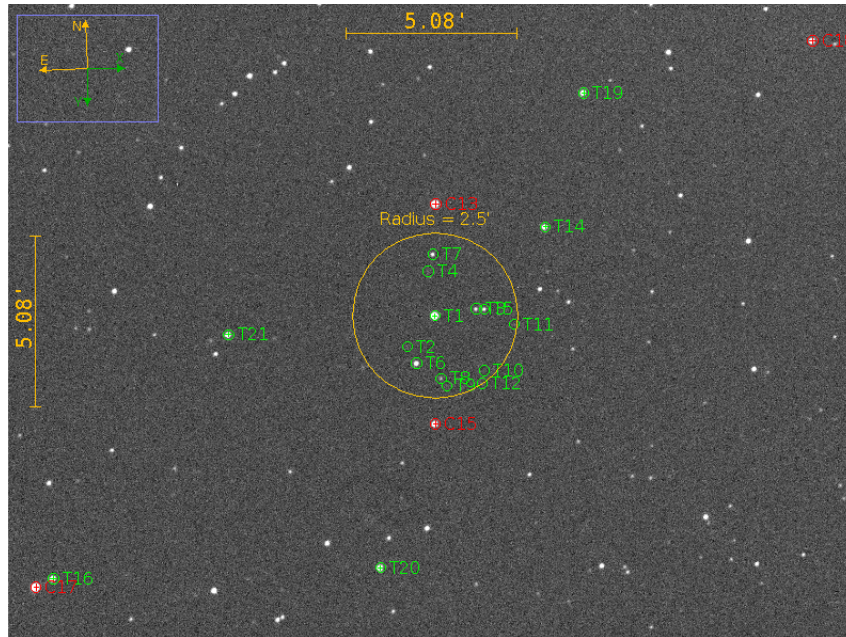


Figure 2.2 An example AIJ field of view. The green annulus labeled "T1" is the target. Red annuli indicate comparison stars, other green annuli indicate stars that were checked for an NEB or near the saturation limit.

has been collected and reduced time series photometry can be performed.

Time series photometry focuses on looking at the flux, or brightness, of stars over time. Before AIJ can perform photometry, it has to know what pixels within the frame to focus on. We do that by placing apertures on the image with radii determined by several factors. One of the main purposes of an aperture is to reduce the noise recorded by AIJ as it measures the flux of the star. The full-width half-maximum of the star's flux is primarily used to determine the aperture radius to ensure that the entire star is included. Some background pixels are typically included as well, as long as it does not introduce a large amount of noise. Since a star's flux can differ from filter to filter, the apertures will also change depending on the filter used. The focus can also be different depending on the filter, and can sometimes vary from night to night, which can also change the size of the aperture used. Once apertures are placed on the target star, they are also placed on any star located within a 2.5 arcminute radius of the target, and then other stars are selected to be used as comparison stars. An

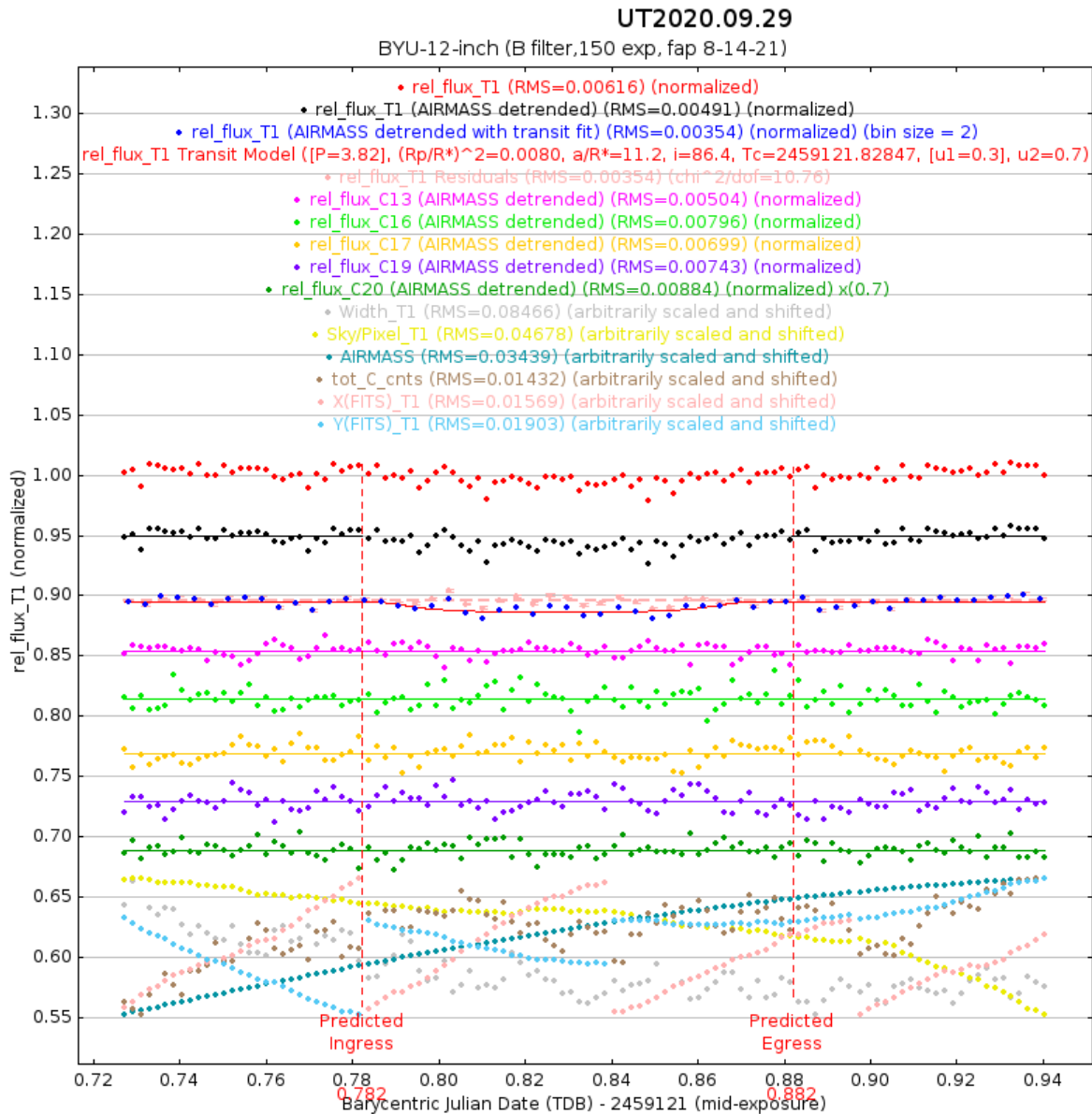


Figure 2.3 An example a plot produced by AIJ. The top three plots originate from the target, with various binning and fitting applied to it. The pink, light green, yellow, purple, and dark green plots are from nearby comparison stars. The rest of the data represents various seeing and sky conditions.

example of an AIJ field of view is shown in figure 2.2.

As mentioned previously, TESS will often assign the observed drop in brightness to the wrong star due to its large field of view. Because of this, SG1 is required to analyze all of the stars within

a 2.5 arcminute radius. By doing this it is assured that the source of the drop in brightness will be found, even if it is not on the star marked as the target. This is one of the main roles of SG1, and is crucial to finding false positives. If a nearby object is the source of the drop in flux then that information is passed along to the main TESS team. Further observations are then needed to determine if the new source is the correct source, and to determine what kind of object it is. It is reassigned to SG1 for those purposes.

In addition to the objects within the 2.5 arcminute radius, comparison stars are needed to help confirm the validity of the transit. Comparison stars are stars that have both a similar brightness to the target star, and a constant brightness, making them ideal to compare to a transit target. They can be used to prove that there is an actual drop in flux occurring, and the transit is not due to an instrumentation error or poor observing conditions. Comparison stars are manually selected based on some of the information given by AIJ. Once reduced image frames have been imported into AIJ, AIJ displays the brightness value for the pixels you are currently hovering over. To choose comparison stars, the brightness of the target star is first noted, and that is used to find stars with a similar brightness. As the comparison stars are being selected, the user checks the brightness value to ensure that it has a similar value as the target. If a particular star does have a similar value it is selected as a comparison star. If there are no stars with a similar brightness value, then stars with smaller brightness values are preferred. Once all of the apertures are placed then AIJ can perform photometry.

AIJ analyzes the brightness of every marked star in every frame and then plots the normalized flux of those stars over time. The barycentric Julian date (BJD) is used for the time (x-axis) as it is preferred by the TESS team. BJD is similar to the Julian Date (JD) in that it is the number of days that have passed since the beginning of what we call Julian time, which began on January 1, 4713 BC. The BJD differs slightly from the JD because it is time as measured at the barycenter, or center of mass, of the solar system where as the JD is measured at earth. Although the difference in time is

small, it is crucial to be consistent with the rest of the TESS team to make data consistent across all science groups.

An example of a plot produced by AIJ is shown in figure 2.3, and as seen in the plot legend, the top three data sets are measurements from the target star. The data in red is raw data with no changes made to it. The data in black has been detrended with respect to the measured air mass and has a flat fit applied to it before and after the calculated transit time. The data in blue is the target data with a transit fit applied to it. AIJ automatically applies a transit fit to the data by reducing the RMS values of the data and fit, and by also using a chi squared method. In simple terms, AIJ assumes that the light curve will have a shape similar to an upside-down top hat. With this assumption AIJ fits a transit with the lowest RMS value possible for the transit itself, and then uses chi squared to fit the ingress and egress. The fourth line of the legend lists a few parameters from the transit fit, one of which being the depth of the transit, which was mentioned in a previous section. The fits produced by AIJ are trustworthy to a reasonable degree, but can be misleading at times. The raw data is also included on this plot for this very reason, it serves as a sanity check for scientists to ensure that AIJ is not fitting a transit that isn't actually there.

The next 5 data sets are from comparison stars. They have been detrended with respect to airmass and have had a flat or constant fit applied to it. As mentioned above, efforts are made to select high quality comparison stars during aperture placement, however, it is hard to know the true quality until photometry is performed. In the legend the RMS value for each comparison star is listed in the legend, with a good comparison star having a RMS value as close to zero as possible. Each comparison star is examined and the lowest RMS values are selected, any with a RMS value close to 0.001 or higher is disregarded. The rest of the data seen in the plot represent various seeing conditions. For instance, if a cloud passed in front of the telescope, we would be able to see that in the seeing and sky conditions and take that into account when analyzing the data. This ensures that any drops in brightness due to observing conditions are accounted for and not mistaken for

a transit or another event. All of these data sets are necessary to help determine whether or not a transit occurs on the target in question.

Chapter 3

Observational Data

Due to the sensitive nature of these observations, publishing the TESS object-of-interest number or the coordinates is not allowed. From this point on the object that was observed and will be discussed will be referred to as simply "the target".

3.1 BYU data

Figures 3.1 and 3.2 show two light curves produced from data from BYU that was gathered on December 7, 2020. Figure 3.1 shows data that was taken in a B filter with a 120 second exposure. Figure 3.2 was taken on the same night in a Sloan z filter also with a 120 second exposure. These plots do not contain the light curves for comparison stars, differing from figure 2.3.

Looking at the seeing conditions at the bottom of the plot, there are a few things to note. We can see that at the beginning of the night the seeing conditions are fairly poor. The sky pixel value is high during the first observations because BYU starts observing during nautical twilight when the sky is not completely dark. As the observations continue throughout the night the sky pixel value gets lower as the sky becomes darker. Airmass, shown in teal on the plot, is extremely important. As the name suggests, airmass measures how much "air" is being observed through, or how many

layers of the atmosphere the telescope is observing through. The closer to the horizon the telescope is pointed, the higher the airmass becomes. For this particular data set the airmass is low at the beginning, but gets larger throughout the night. This means that the telescope started observing this object when it was higher in the sky, and much closer to the meridian. Then, over time, the target began to set, meaning the telescope was observing through more layers of the atmosphere and the airmass value went up. This is important data to gather as astronomical data typically has more noise when the airmass is higher, which can factor into data analysis.

Other important aspects of this plot are the light blue and light pink curves, which change periodically throughout the night. Those two curves are the Y-position and X-position of the target in the field of view. This telescope at BYU does not have guiding like many other telescopes. Throughout the night the target will drift slightly, and then the telescope will recenter, creating the positional shifts seen in the plots. This, unfortunately, can be the cause of some noise as the target will occasionally appear "smeared" in the images. It also forces AIJ to rely on plate solving and it's own tracking to ensure that the target is always inside of the annulus. AIJ is often very reliable and accurate while doing this, but it can make small errors, causing some noise in the data.

Now, changing the focus to the red curve, which is the light curve from the target with a transit fit applied to it. Both plots show that a transit fit was successfully fitted to the data, indicating that a transit did occur on this target. However, the exact shape and depth of this target could be different from what we see here, as there is some uncertainty in the data. This is indicated by the error bars on the data points. Taking those errors into account, we can determine visually that it is very possible for the transit in 3.2 to be much shallower or much wider than the fit implies. The fit in figure 3.1 seems to fit the data better through visual inspection.

It appears as though the observed transit time was slightly different than expected. The predicted times are indicated by the vertical, pink, dotted lines in the plot, and the ingress occurs close to the predicted time, but the egress occurred before the predicted time. This indicates that the predicted

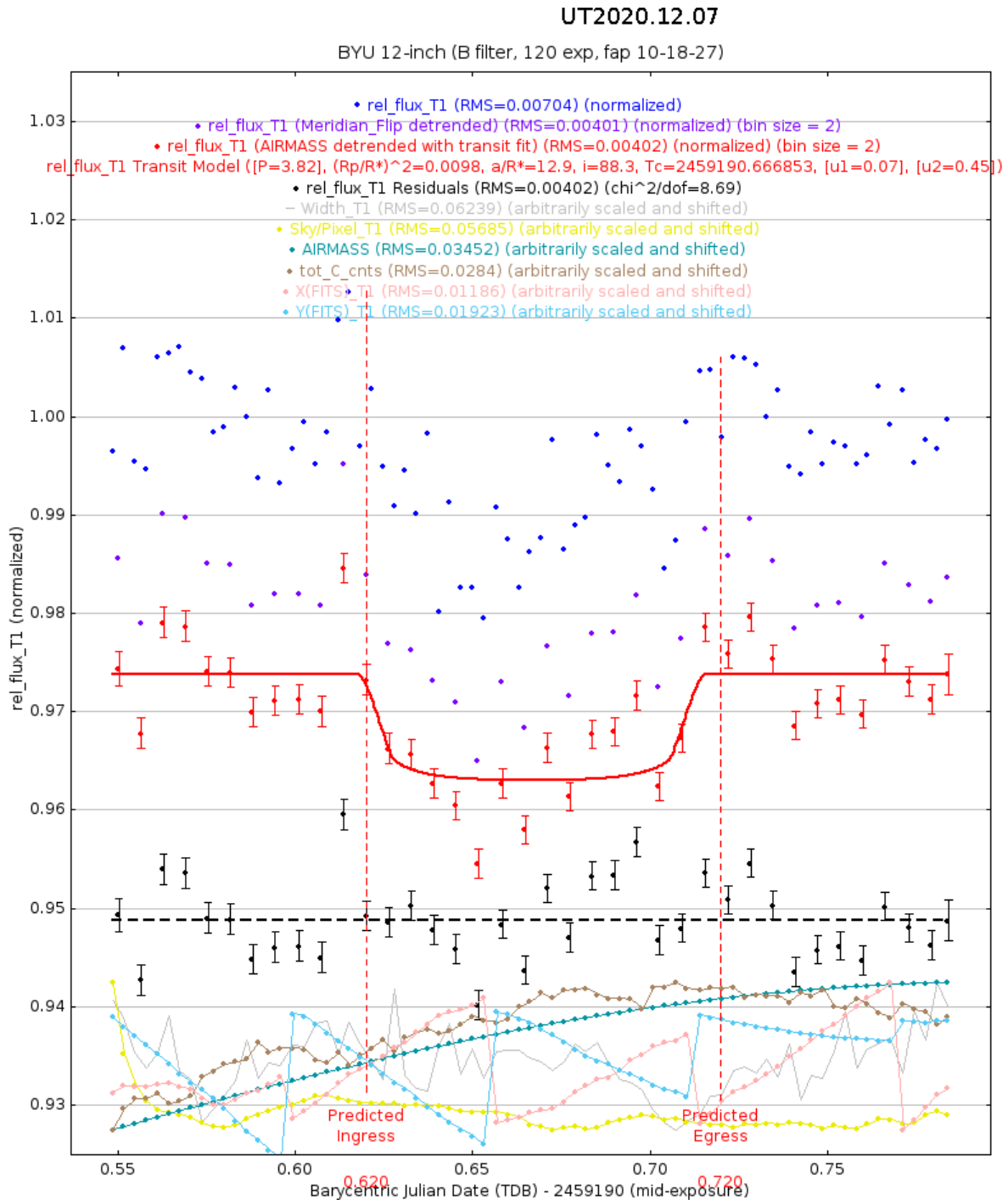


Figure 3.1 Light curve plot produced with AIJ, based from December 7, 2020, taken at BYU in a Johnson B filter. The top three data sets in dark blue, purple, and red show the transit data, with a transit fit applied to the red data. This has the characteristic shape of a planet transit, and shows that the transit ended earlier than expected.

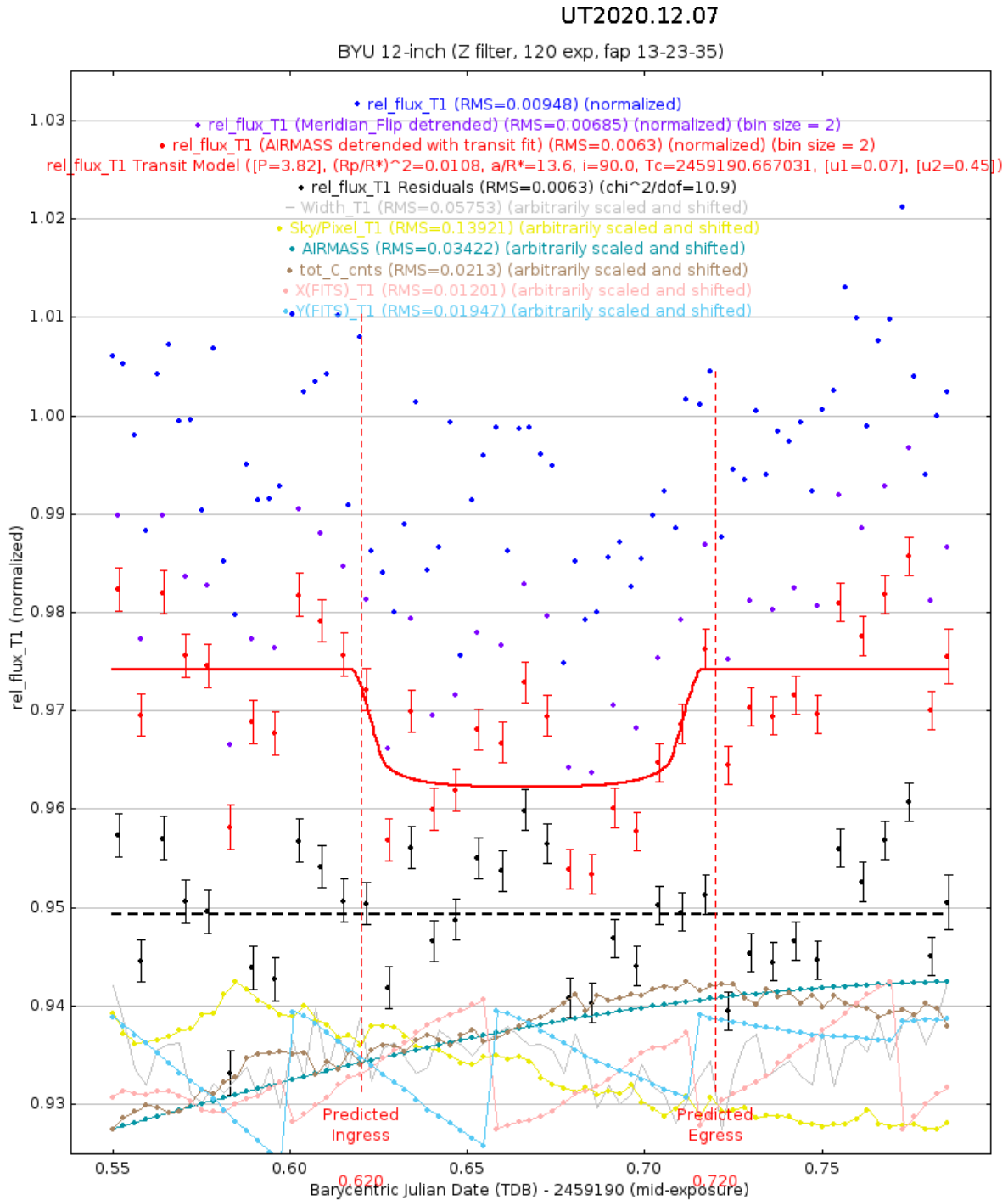


Figure 3.2 Light curve plot produced with AIJ, based from December 7, 2020, taken at BYU in a Sloan z filter. The top three data sets in dark blue, purple, and red show the transit data, with a transit fit applied to the red data, however there is a large amount of uncertainty in this data set. The fit shows the characteristic shape of a planet transit and that the transit ended earlier than expected.

transit duration is longer than the observed transit. Knowing the observed ingress and egress times is extremely helpful, as that data can help us calculate more precise transit times in the future, resulting in more accurate observations and analysis.

Data was gathered at BYU on two additional nights and the resulting light curves can be found in appendix A. Figure A.1 shows data from September 6, 2020. The transit started much earlier than calculated and as a result, the egress was only a short time after the predicted ingress time. However the length of the transit looks to be as predicted. The error bars seen on this data are smaller than the error bars seen on figure 3.4 indicating that this transit fit is slightly more trustworthy than the transit fit seen in figure 3.2 because the transit depth and shape is more significant than the errors. That being said, looking at the raw data in purple, it is fairly noisy, so the exact timing and shape of the transit may be slightly different than shown by the transit fit.

The last set of observational data is shown in figure A.2 and the data was collected on September 29, 2020. Looking at the transit fit, it came on time or slightly late and it also ended slightly earlier than expected. As was the case in the previously discussed plot, the errors are smaller on this plot meaning that the transit model can be trusted. However, both the transit fit and the raw data is slightly more v-shaped. This can be an indication of the target being an eclipsing binary instead of a transiting planet. This possibility will be explored in a later section.

3.2 ExoFop Data

As mentioned previously, data was taken at other observatories around the world and was accessed through the ExoFOP data base. Data taken at LCO-McD was taken in Sloan Z and Johnson B filters, the same filters used at BYU. The light curves for these observations are shown in figures A.6 and 3.4. LCO-McD was able to gather very high quality data with low uncertainty, as indicated by the small error bars. The sky conditions for these observations were also very good, which likely helped

improve the quality of the data. The light curve produced from the data in the Z filter clearly shows a transit that is within the error bars. The light curve in the B filter also shows a transit fit, but the transit appears shallower and with more outliers. Both of these light curves show that the transit timing is different from predicted, and the actual transit may start and end later than expected, or is shorter than expected.

Data from OPM was taken in two filters, the same z filter as BYU and LCO-McD, as well as a Sloan g filter. These light curves are found in appendix A, figures A.4 and A.3. The Sloan g filter has a central wavelength of 477 nm, and is bluer than the Johnson B filter. The light curves produced with the OPM z data seen in figure A.4 is visually similar to the BYU data taken in the same filter. They both have similar depths of 0.02 and very similar shapes, but the OPM data shows a much shorter transit than BYU. This timing difference may be due to the amount of uncertainty in the OPM data. It has much larger error bars, many of which are larger than the overall depth of the transit. It is possible that the overall timing of the transit seen by OPM is actually similar to the BYU data, but AIJ could not find an accurate fit due to the uncertainty of the OPM data. The g filter light curve from OPM is shown in figure A.3. In this filter the depth is about the same, but the timing is very different from the timing seen in the z filter. The observed transit duration is almost the exact same as the calculated transit duration, but the ingress and egress times are slightly different. The uncertainty of the data in this filter is smaller, which implies that the data and fit are more trustworthy overall.

The light curve from Cal'Ou in figure 3.5 shows a transit fit, but there are some outliers in the data. The raw data does have a visible drop in it, but it does not have the typical transit shape. It is more V-shaped and not a square light curve that is characteristic of a transiting planet. This could be an indication that this target is an EB, but more data is needed to come to a concrete conclusion. The timing of the transit is similar to the timing of other data sets, which may indicate that the observed timing is more accurate than the calculated timing and it needs to be adjusted. Correcting

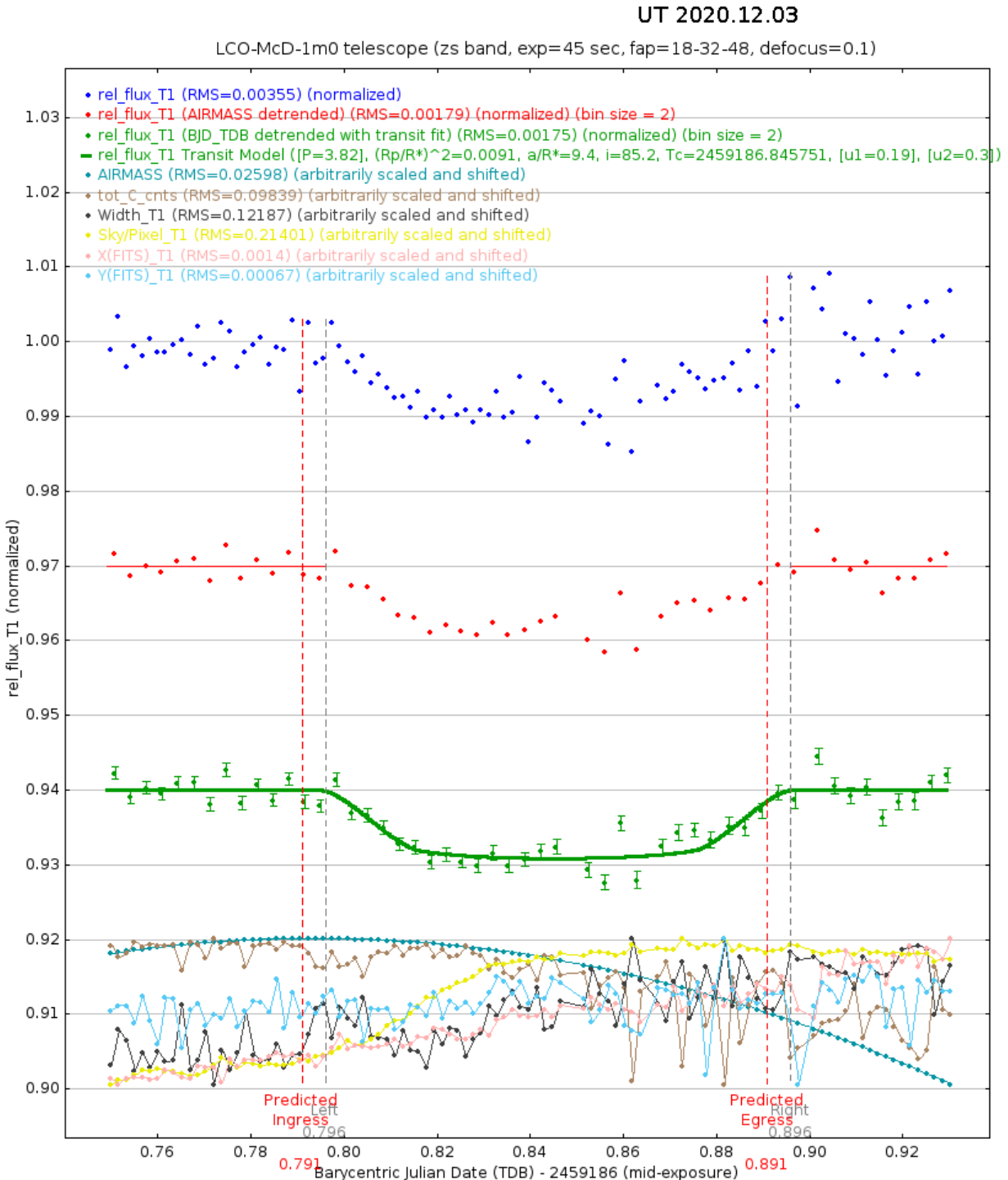


Figure 3.3 This plot was produced using AIJ and displays the data that was gathered by LCO-McD on December 3, 2020 with a Sloan z filter. The dark blue, red, and green data show the normalized flux of the target overtime, with a transit fit applied to the green data. This data shows a shallower transit than other data sets, but a transit is still evident. From the vertical dashed lines the transit seems to have started and ended later than expected.

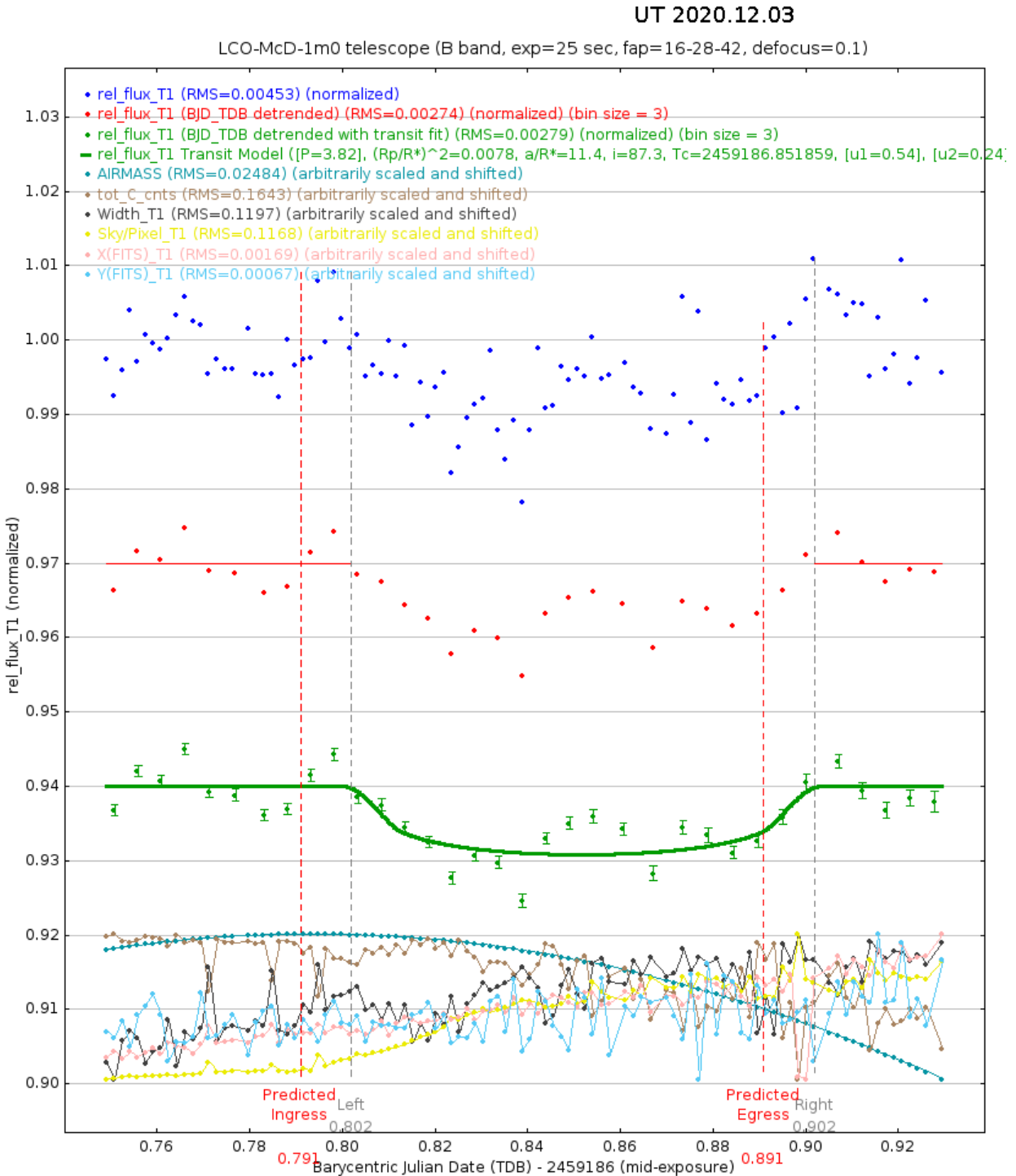


Figure 3.4 This plot was produced using AIJ and displays the data that was gathered by LCO-McD on December 3, 2020 with a Johnson B filter. The dark blue, red, and green data show the normalized flux of the target overtime, with a transit fit applied to the green data. This data shows a shallower transit, more rounded transit when compared to other data sets, but the transit still appears to be from a planet.. From the vertical dashed lines the transit seems to have started and ended later than expected.

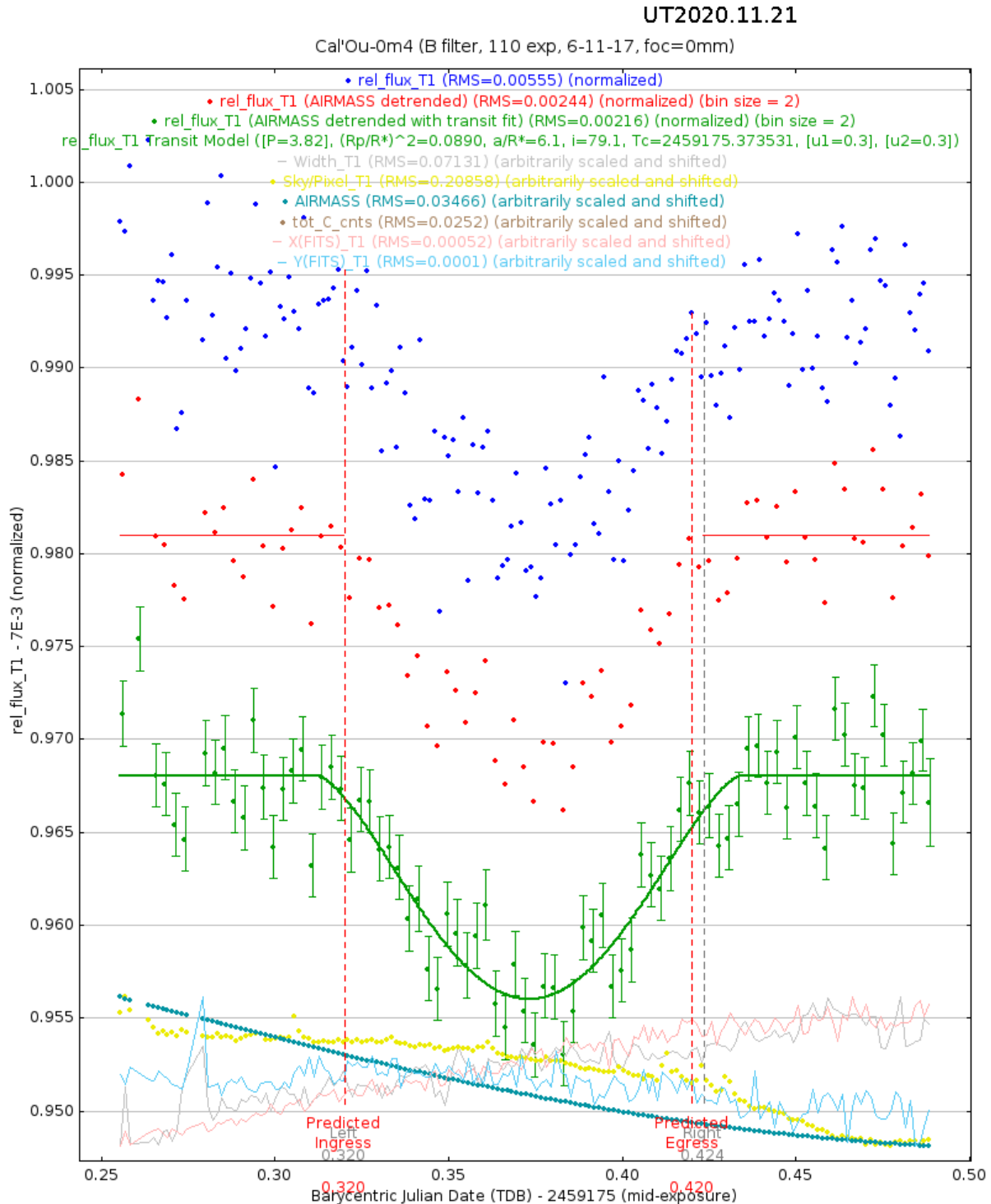


Figure 3.5 This plot was produced using AIJ and displays the data that was gathered by Cal'Ou on November 23, 2020 with a Johnson B filter. The dark blue, red, and green data show the normalized flux of the target overtime, with a transit fit applied to the green data. This transit has a more V-shaped transit, which can indicate an EB, but not always. Although this transit appears to have a greater depth, it has a similar value to the other light curves presented.

system properties like the transit timing is one of the roles of SG1 and is crucial for both future observations, and eventually determining what kind of object the target is. The data from V39 is presented in figure A.5. This data was taken in the Johnson B filter, which was also used by BYU and LCO-McD. Despite using the same filter, the data is noticeably different. The transit fit on the green data points seems very reasonable as the error bars do not exceed the depth of the transit, and the transit fit visually matches the raw data. Because of the differing transit shapes seen in this data there is a need for additional observations and modeling.

Chapter 4

Modelling with EXOFASTv2

4.1 EXOFASTv2

EXOFASTv2 (Eastman et al. 2019) is a highly advanced transit modeling software which runs within the Interactive Data Language (IDL). It is capable of modeling an arbitrary number of planets based off of observational data. The data required includes the BJD times, the normalized flux, and the normalized flux errors of the host star, all of which are easily produced by AIJ. This data is stored in the AIJ measurements table and is then transferred into a new file that contains only the necessary data and is in a format that is readable by IDL. EXOFAST also requires some system parameters, such as the orbital period, the effective temperature, mass, and radius of the host star, as well as the parallax or distance measurement and other values. Most, if not all, of these parameters are provided by the TESS team and then put into a “priors” file that is used by EXOFAST to complete the fit. Once all of the data has been gathered, example files are utilized and modeling can begin. EXOFAST utilizes the Markov Chain Monte Carlo (MCMC) sampling method to create an accurate fit. The user is able to specify how many steps EXOFAST takes to find a satisfactory fit, the priors file to be used, and other fitting parameters. When first starting a fit, it is crucial to first

evolve the priors file. EXOFAST takes the priors file that is first produced by the user and updates it during each run based on the transit fit that was just produced. Overtime the priors should become more and more accurate, so it should be evolved for some time. The main way to check for good priors is to check the chain plot that is automatically produced by EXOFAST. The chain plot (as shown in figure whatever) is an indication of how well the MCMC method is working.

The MCMC method creates several “chains” as it runs, and these chains indicate how probable and accurate the model is. Evolving the priors may take several attempts depending on the quality of the initial priors. For example, in this research, the priors files were updated up to 17 times before good chains were achieved. Figure 4.1 shows the chains used for MCMC for the data from BYU, 09/09/2020. This plot is visually very messy, but this is a good thing. When the chains become messy it means that there is no long term evolution happening and the priors file had been evolved enough. At this point and modeling was ready to be conducted on this object and a final, extended run was conducted. These runs took at least 50,000 steps and ran for up to 4 hours. After which several plots are created automatically by EXOFAST which model the transit based on the observational data of the target. These models take various things into account, such as limb darkening and can handle a variety of transit shape, making EXOFAST a reliable program for producing transit models for most kinds of systems.

4.2 Transit Models

A transit model was created for each data set. Figure 4.2 shows the models from 4 different data sets, with 6 additional models shown in figure B.1 in appendix B. The upper left plot of figure 4.2 shows the model that was found for BYU data taken on December 7, 2020 in the Sloan z filter. This particular model was produced after the priors file was evolved seven times, and EXOFAST was allowed to take 50,000 steps over the course of roughly 3.5 hours. In the plot the transit model is

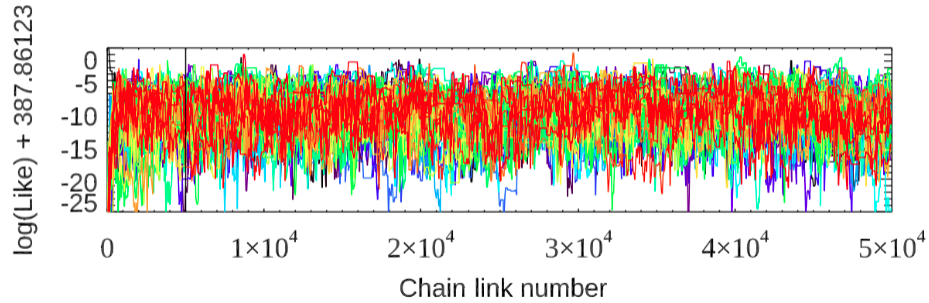


Figure 4.1 Each color represents a chain. Only links to the right of the vertical black line are kept and used when making the model. Generally, we are looking for a lack of long-term evolution to the right of the black line, as well as agreement among all chains. Caption adapted from (Eastman et al. 2019).

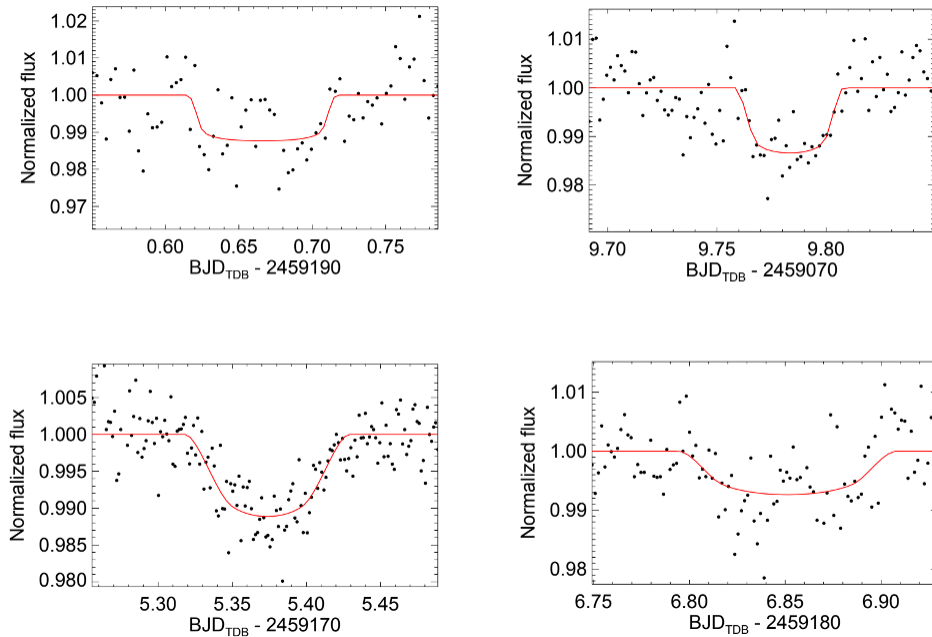


Figure 4.2 4 transit models produced by EXOFAST. The upper left is based on data taken on December 7, 2020 in the Sloan z filter at BYU. The bottom left model is based on data recorded on November 23, 2020 in the Johnson B filter at Cal'Ou. The top right model was based on data recorded on August 18, 2020 in the Cousins I filter at V39. The bottom right model was based on data recorded on December 3, 2020 in the Johnson B filter at LCO-McD. All of which show transit shapes typical of a transiting planet.

shown with the red line, and the observational data is overlaid on top of the model. In addition to creating transit plots, EXOFAST outputs many different system parameters that were found during the modeling process. Some parameters of interest are listed in the table below. Modeling results are shown for the transit that occurred on September 6, 2020, but those results were later thrown out due to the large errors, and hence not included in calculating the average values.

Using the values in the table, the average radius for the transiting object was found to be 1.36 Jupiter radii. This is a plausible planet size, as seen in figure 1.3. This radius also much too small to be a star, implying that this target may actually be a transiting planet, and not an EB as hypothesized in a previous section. The average depth is about 0.001, which is small, but detectable. A small depth such as this implies that the change in flux is due to a small transiting object such as a planet, and not a star.

Observatory	Date Obs. (UT)	Filter	Radius (R_J)	R error	Depth	Depth error
BYU	09/09/2020	Johnson B	1.092	± 0.085	0.00645	± 0.0011
BYU	12/07/2020	Johnson B	1.41	± 0.44	0.017	± 0.0056
BYU	12/07/2020	Sloan z	1.16	± 0.25	0.0074	± 0.0035
LCO-McD	12/03/2020	Johnson B	1.099	± 0.03	0.00679	± 0.0035
LCO-McD	12/03/2020	Sloan z	1.189	± 0.061	0.00765	± 0.00076
V39	08/18/2020	Cousins I	1.54	± 0.15	0.0129	± 0.0019
Cal'Ou	11/23/2020	Johnson B	1.232	± 0.071	0.00389	0.00094
OPM	10/29/2020	Sloan z	1.82	± 0.31	0.0144	± 0.0041
OPM	10/29/2020	Sloan g	1.7	± 0.71	0.0153	± 0.0076
BYU	09/06/2020	Johnson B	1.04	± 1	0.0057	± 0.005

Another aspect of the transit depths to note is how similar all of the depths are, despite much of the data having been collected in different filters. If this was object is a binary system then it is very likely that the chromaticity of the stars would change the transit depth when observed in

different filters. Since different kinds of stars may be emitting, for instance, more infrared light, that star would appear slightly brighter when using an infrared filter, such as the Cousins I filter. If the transiting object is a star then it is likely that the transit depth would be shallower in a certain filter that corresponds to where within the electromagnetic spectrum the star peaks. Since all of the depths are very similar regardless of filter then that increases the chances of this object being a transiting planet and not an EB system.

Chapter 5

Results and Discussion

5.1 Final Results

As a result of this research, 10 different light curve plots, and 10 different transit models have been produced. From this data we are able to conclude that this object is most likely a transiting planet. Almost all of the light plots presented in this paper showed transit shapes that are consistent with a transiting planet, as seen in the bottom of figure 1.6. Transits typically have a square, or U-shaped dip and those shapes are seen in almost every light curve plot. An especially good example of a typical transit shape can be seen in figure 3.2. There is, however, one light curve plot that has a shape that is not typical of a transiting planet. Figure 3.5 displays the data from Cal'Ou, which has a more V-shaped curve as opposed to a U-shaped curve. This shape can indicate that this target is an EB instead of a planet.

The models provide further evidence that this target is a planet. All of the models show transit shapes that are very typical of a planet. The top most plots in figure B.1 both show transits that are U-shaped, and are hence indicative of a planet. The bottom left plot in figure 4.2 is the model produced based on the data from Cal'Ou. As mentioned above, the light curve is V-shaped, but the

model is more U-shaped. Based on the flux measurements from Cal'Ou, EXOFAST found that a planet transit fit the data better than the V-shaped fit found by AIJ. As discussed in the previous section, EXOFAST also found system parameters for this target, and found that the radius of the transiting object is only slightly bigger than Jupiter. It is extremely unlikely for a star to have a radius similar to Jupiter's, so this is most likely a planet. EXOFAST also found that the depth is fairly consistent across all data sets, despite the variety of filters. This implies that the object does not change color when looking in different filters. Hence, the object is more likely to be a planet, and not a star, which can look different when using different filters. This further supports the conclusion that this target is a planet, but variety of observations are needed to confirm this conclusion

5.2 Future Observations

More observations and study on this target would be beneficial to determine what if this target is indeed a planet. More photometric data would be helpful, as it could be used to confirm the findings in this thesis. This could be completed by BYU or other observatories that are apart of SG1. These observations could also help the TESS team derive improved transit ingress and egress times. Observations could also be performed using a greater variety of filters in order to check for any chromaticity, and hence changes in transit depth with the changes in filter. Once SG1 is able to gather more photometric data then further modeling can be performed, which could reinforce the results found here. Some other observations that can be done are spectroscopic observations. These could be done by SG2, and would confirm that the target is not an EB by showing a single stellar spectrum, and not a blended spectrum . If the target and its companion is massive enough spectroscopic data might also show a Doppler shift, which can be used to find stellar properties for this system.

In addition to the data collection from SG1 and SG2, SG3 could also be used to gather more data for this target. They specialize in direct imaging, by using the adaptive optics that are available at the Keck Observatory in Hawaii. SG3 is capable of spatially resolving objects such as this in order to determine if there are two bright objects next to each other, such as an EB. They do this by resolving the object to the best of their ability, and then checking for any asymmetries in the images. If there is an asymmetry then it indicates that there are two or more stars orbiting each other, instead of a planet orbiting a star. More data from various science groups would be extremely helpful in determining whether this target is a planet, as the data presented here suggests, or if it is another objects, such as an EB.

Appendix A

Additional Light Curves

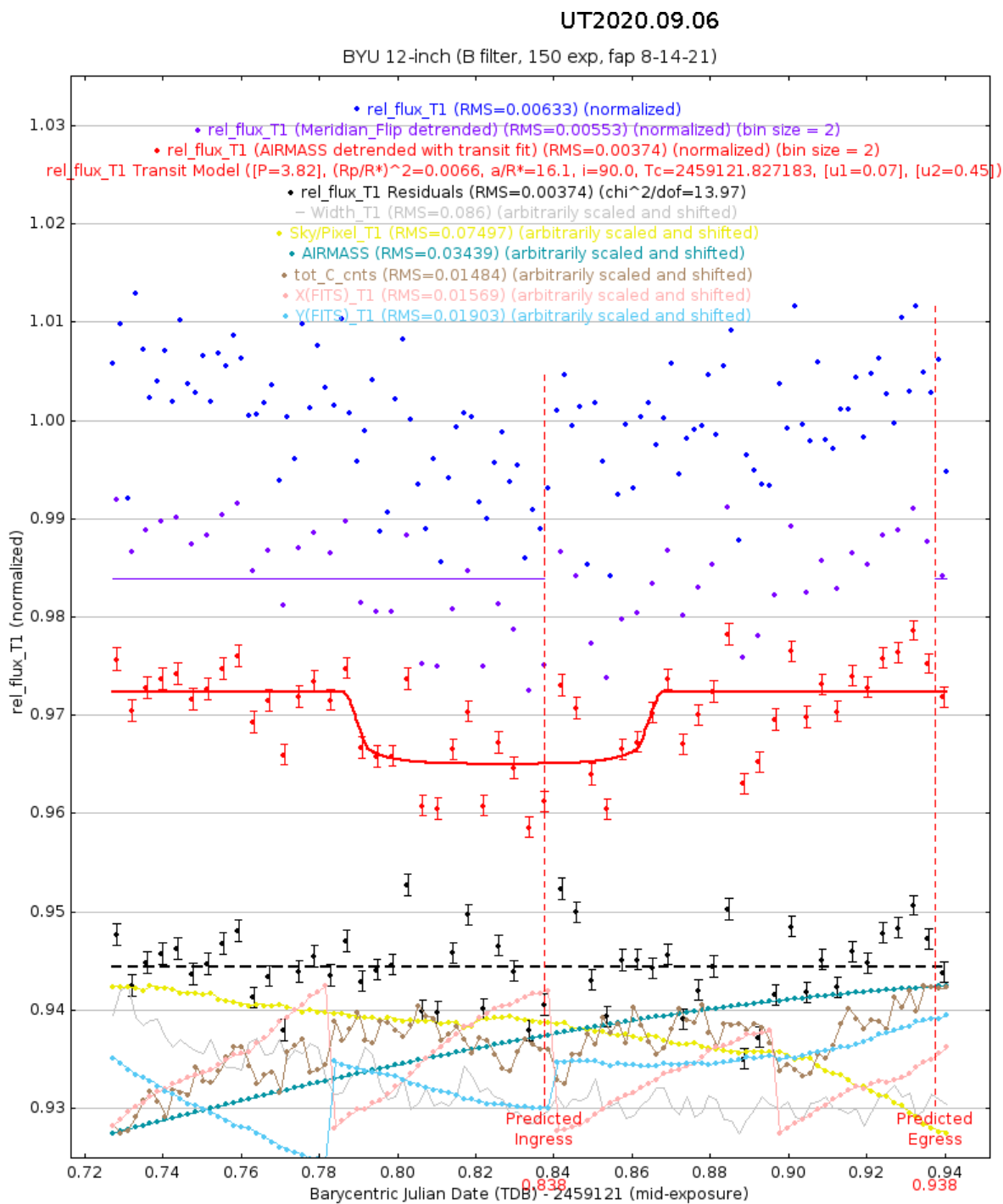


Figure A.1 This plot was produced using AIJ and displays the data that was gathered by BYU on September 6, 2020 with a Johnson B filter. The dark blue, purple, and red data show the normalized flux of the target overtime, with a transit fit applied to the red data. This data shows a square-shaped transit that appears to be from a planet. From the vertical dashed lines the observed transit timing was very different from the calculated transit time.

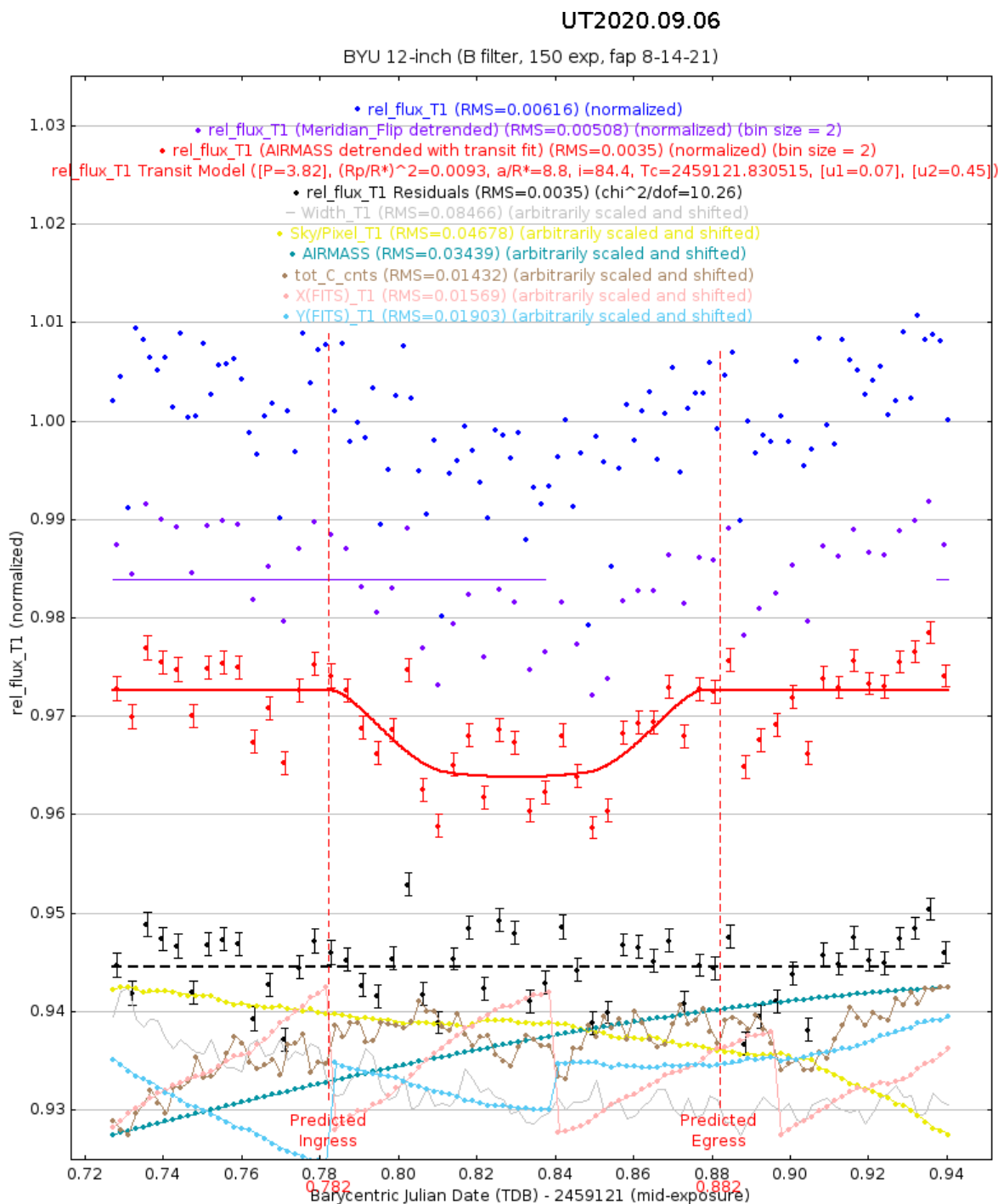


Figure A.2 This plot was produced using AIJ and displays the data that was gathered by BYU on September 9, 2020 with a Johnson B filter. The dark blue, purple, and red data show the normalized flux of the target overtime, with a transit fit applied to the red data. This data shows a more U-shaped transit that could be from a transiting planet. From the vertical dashed lines the observed transit timing was fairly similar to the calculated times, but the transit may have ended earlier than expected.

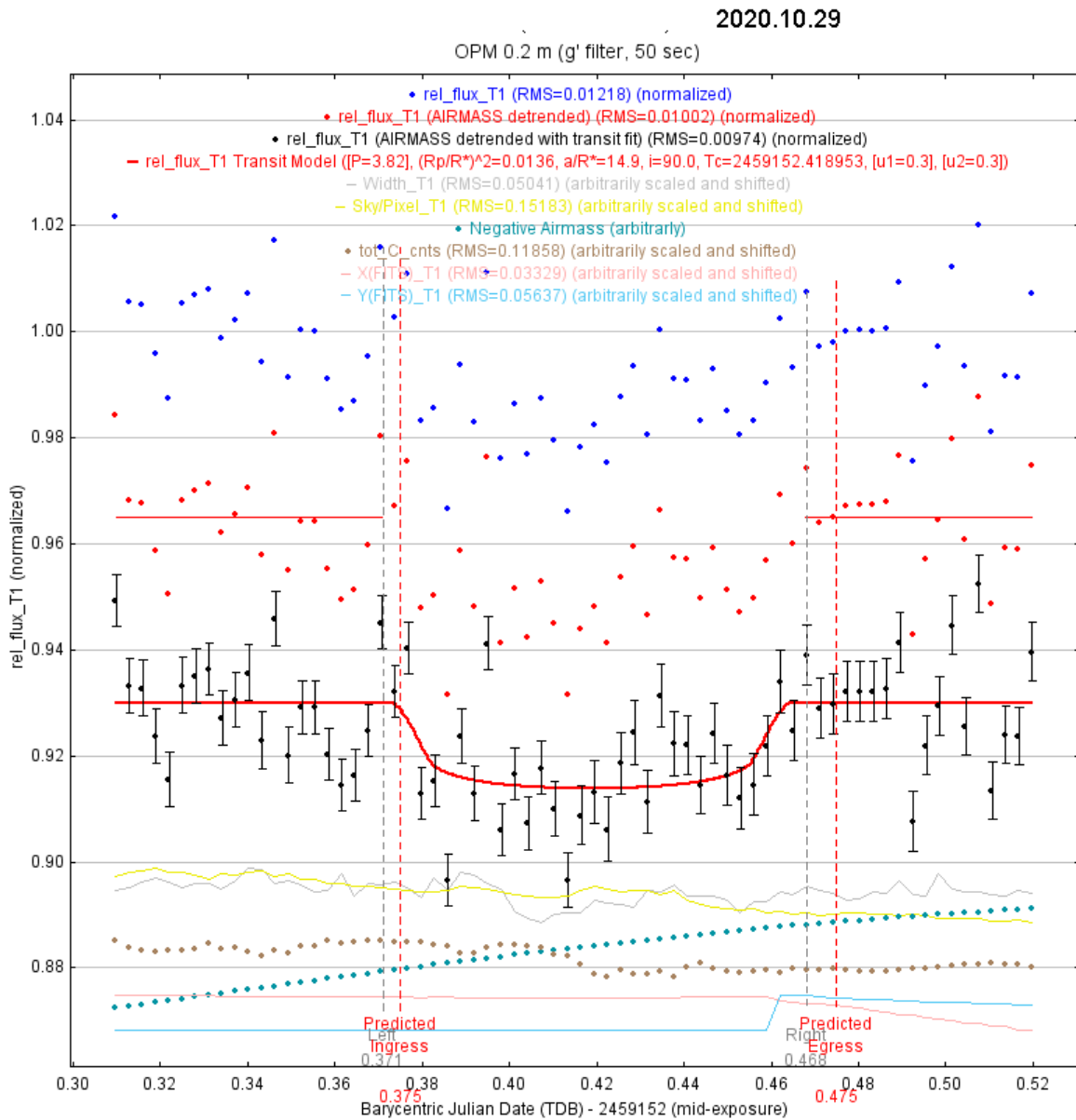


Figure A.3 This plot was produced using AIJ and displays the data that was gathered by OPM on October 29, 2020 with a Sloan g filter. The dark blue, red, and black data show the normalized flux of the target overtime, with a transit fit applied to the black data. From the vertical dashed lines the transit seems to have started and ended earlier than expected

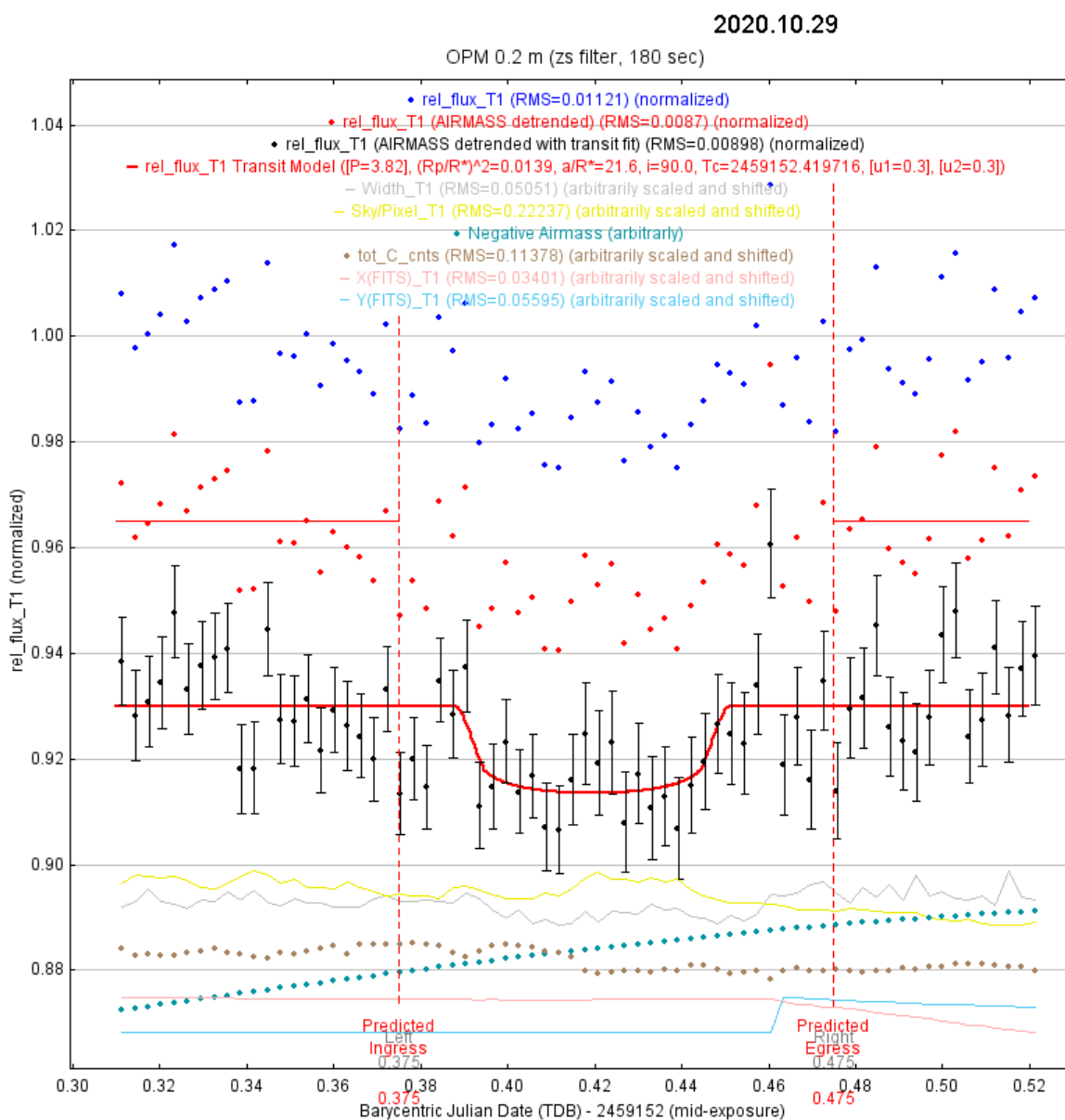


Figure A.4 This plot was produced using AIJ and displays the data that was gathered by OPM on October 29, 2020 with a Sloan z filter. The dark blue, red, and black data show the normalized flux of the target overtime, with a transit fit applied to the black data. This data has a higher uncertainty than other data sets based on the error bars, but a transit is still plausible. Based on the vertical dashed lines the transit seems to have started and ended earlier than expected

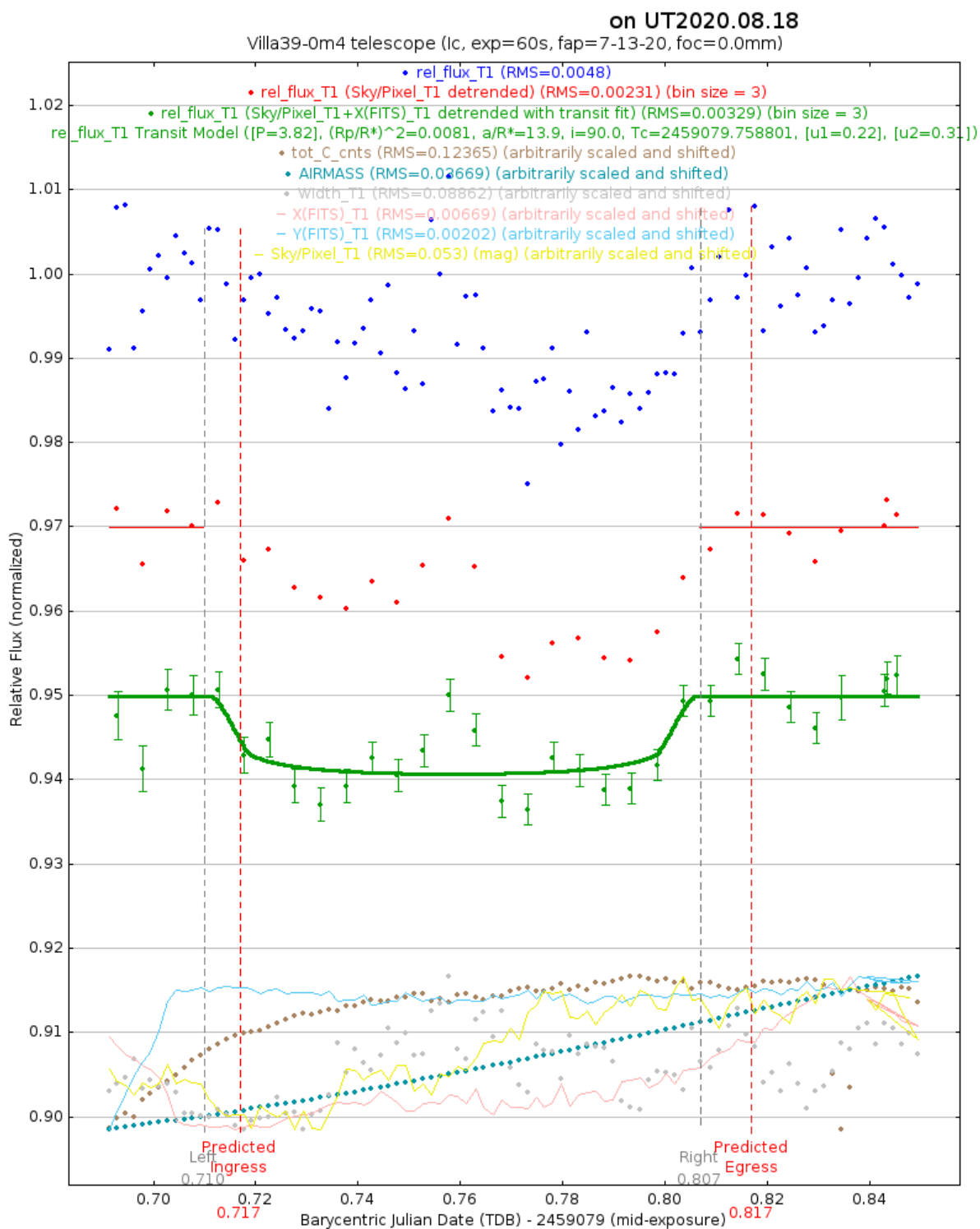


Figure A.5 This plot was produced using AIJ and displays the data that was gathered by V39 on August 18, 2020 with a Cousins I filter. The dark blue, red, and green data show the normalized flux of the target overtime, with a transit fit applied to the green data. Based on the vertical dashed lines the transit seems to have started and ended earlier than expected

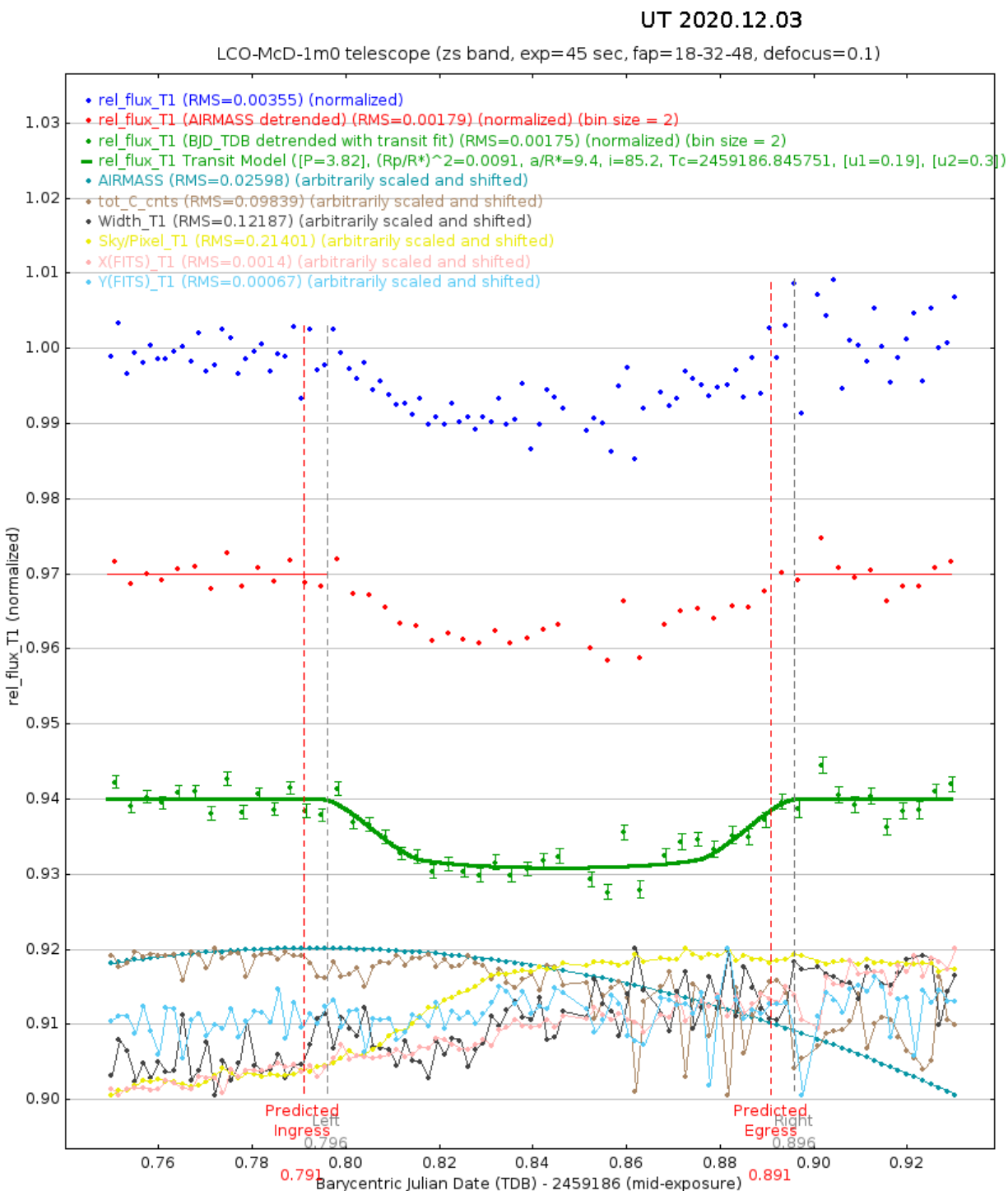


Figure A.6 This plot was produced using AIJ and displays the data that was gathered by LCO-McD on December 3, 2020 with a Sloan z filter. The dark blue, red, and green data show the normalized flux of the target overtime, with a transit fit applied to the green data. Based on the vertical dashed lines the transit seems to have started and ended slightly later than expected

Appendix B

Additional Transit Models

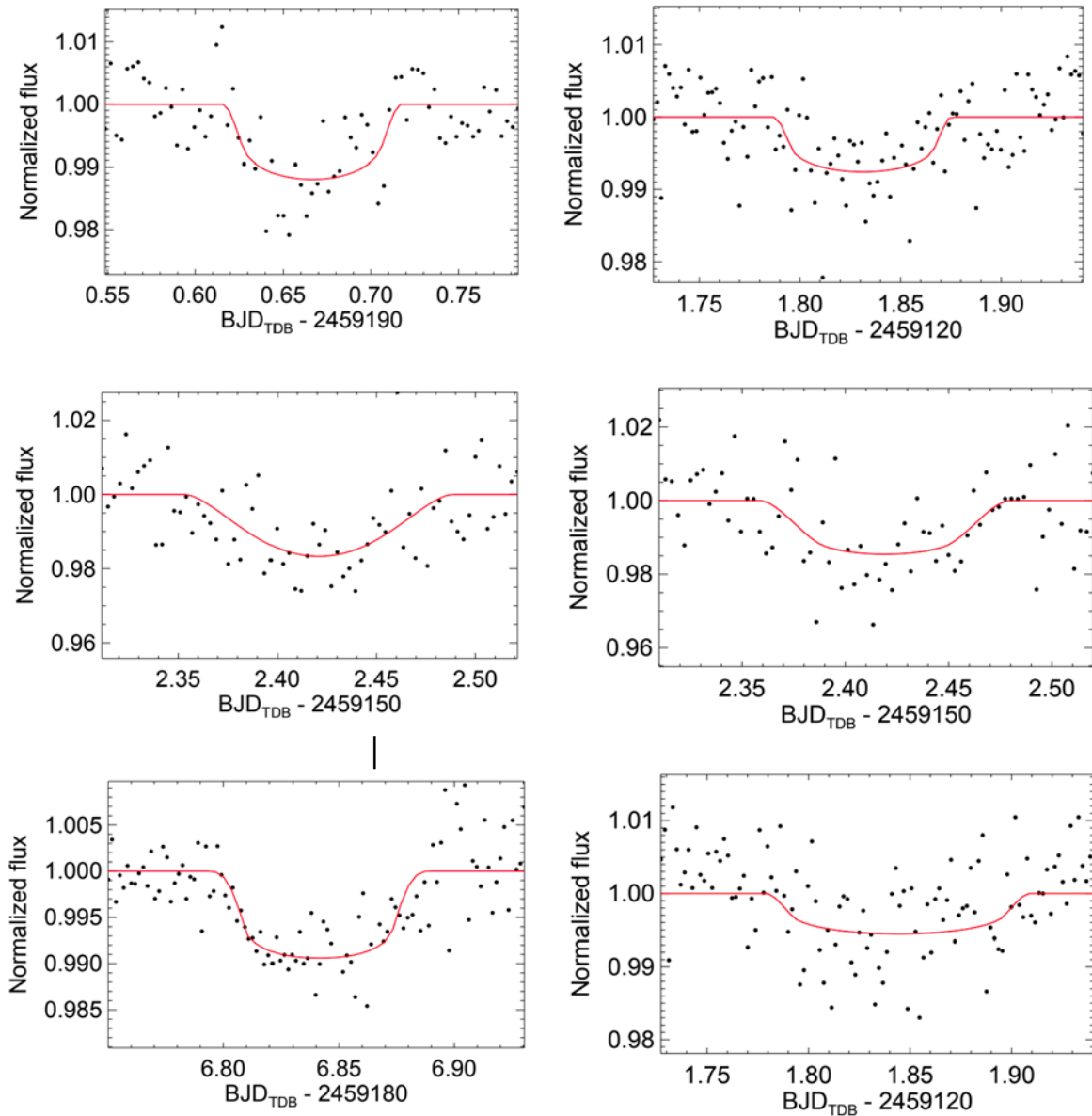


Figure B.1 6 transit models produced by EXOFAST. The upper left is based on data taken on December 7, 2020 in the Johnson B filter at BYU. The upper right is based on data taken on September 9, 2020 in the Johnson B filter at BYU. The middle left is based on data taken on October 29, 2020 in the Sloan z filter at OPM. The middle right is based on data taken on October 29, 2020 in the Sloan g filter at OPM. The lower left is based on data taken on December 3, 2020 in the Sloan z filter at LCO-McD. The lower right is based on data taken on September 9, 2020 in the Johnson B filter at BYU. The lower right model had very large uncertainties associated with it, and should not be considered to be an accurate model. All other models can be considered accurate models and show transit shapes that are consistent with transiting planets.

Bibliography

Accessed April 10, 2022, <https://www.aavso.org/filters>

Accessed April 10, 2022, <http://slittlefair.staff.shef.ac.uk/teaching/phy217/lectures/instruments/L12/index.html>

Akeson, R., & Christiansen, J. 2019, in American Astronomical Society Meeting Abstracts, Vol. 233, American Astronomical Society Meeting Abstracts #233, 140.09

Batalha, N. M., et al. 2013, ApJS, 204, 24

Bessell, M. S. 2005, ARA&A, 43, 293

Brown, T. M., et al. 2013, PASP, 125, 1031

Canas, C. I. Accessed April 10, 2022, <https://hpf.psu.edu/2020/09/15/toi-1899/>

Ciardi, D. 2019, in American Astronomical Society Meeting Abstracts, Vol. 233, American Astronomical Society Meeting Abstracts #233, 140.07

Collins, K. 2019, in American Astronomical Society Meeting Abstracts, Vol. 233, American Astronomical Society Meeting Abstracts #233, 140.05

Collins, K., Quinn, S. N., Latham, D. W., Christiansen, J., Ciardi, D., Dragomir, D., Crossfield, I.,

& Seager, S. 2018, in American Astronomical Society Meeting Abstracts, Vol. 231, American Astronomical Society Meeting Abstracts #231, 439.08

Collins, K. A., Kielkopf, J. F., Stassun, K. G., & Hessman, F. V. 2017, AJ, 153, 77

Copied From Dawson, R. I. 2020, AJ, 159, 223

Copied From NASA-Ames,. Accessed May 10, 2021, https://www.nasa.gov/mission_pages/kepler/multimedia/images/transit-light-curve.html

Copied From Nasa-Ames, & Wendy Stenzel,. Accessed April 10, 2022, https://www.nasa.gov/mission_pages/kepler/multimedia/images/kepler-skittles-bars.html

Copied from NASA-Ames, & Wendy Stenzel,. Accessed April 10, 2022, <https://www.nasa.gov/feature/ames/kepler/briefingmaterials160510>

Copied From the NASA-Exoplanet-Archive,. Accessed April 13, 2022, <https://exoplanetarchive.ipac.caltech.edu/exoplanetplots/>

Copied From the TESS website,. Accessed May 10, 2021, <https://tess.mit.edu/>

Dragomir, D., Latham, D. W., Collins, K., Quinn, S. N., Ciardi, D., Christiansen, J., Crossfield, I., & Seager, S. 2019, in American Astronomical Society Meeting Abstracts, Vol. 233, American Astronomical Society Meeting Abstracts #233, 140.08

Eastman, J. D., et al. 2019, arXiv e-prints, arXiv:1907.09480

Latham, D. W. 2019, in American Astronomical Society Meeting Abstracts, Vol. 233, American Astronomical Society Meeting Abstracts #233, 164.06

Quinn, S. N. 2019, in American Astronomical Society Meeting Abstracts, Vol. 233, American Astronomical Society Meeting Abstracts #233, 140.06

Ricker, G. R., et al. 2014, in Society of Photo-Optical Instrumentation Engineers (SPIE) Conference Series, Vol. 9143, Space Telescopes and Instrumentation 2014: Optical, Infrared, and Millimeter Wave, ed. J. Oschmann, Jacobus M., M. Clampin, G. G. Fazio, & H. A. MacEwen, 914320

Shames, P., & Tody, D. 1986, A User's Introduction to the IRAF Command Language (NOAO)

Spencer, A. Brigham Young University, Provo, UT 2019, Thesis Archive